Australian Government
Department of Defence
Defence Science and
Technology Organisation

Assessment of TEM Cells for Whole Aircraft EMV Testing

Andrew J. Walters and Chris Leat

Air Operations Division

Defence Science and Technology Organisation

DSTO–RR–0149

ABSTRACT

Transverse Electromagnetic (TEM) cells offer one solution to the problem of electromagnetic vulnerability (EMV) testing of whole vehicles at lower frequencies. Combined with a reverberation chamber (RC) TEM cells offer an attractive solution to a EMV testing facility which could operate in the frequency range of 10 kHz to 18 GHz. In order to move toward a hybrid RC/TEM facility the non-uniform transition region between TEM and RC operation (i.e. 17 MHz to 30 MHz) must be addressed. This report discusses computational electromagnetics (CEM) modelling used to characterise the DSTO scale TEM cell. The cell was built with the aim of integrating a full scale version into the DSTO RC. The CEM model of the TEM cell was validated using measurements, which showed good agreement. It was then assessed for applicability for aircraft EMV testing by comparing a simulated aircraft in the cell against an aircraft on an Open Area Test Site (OATS) and in free space. The work highlighted the need for resonance suppression in the transition region. We introduce a novel way of active resonance suppression and demonstrate its effectiveness when applied to the first TE resonance. Finally the feasibility of integrating a TEM cell into the DSTO RC is discussed including costs for major items

Published by

Defence Science and Technology Organisation
PO Box 1500
Edinburgh, South Australia 5111, Australia

Telephone: (08) 8259 5555
Facsimile: (08) 8259 6567

AR No. 013-897
May 2007

APPROVED FOR PUBLIC RELEASE

Assessment of TEM Cells for Whole Aircraft EMV Testing

Executive Summary

Avionics systems have the potential to suffer from undesirable behaviour when exposed to radio frequency (RF) energy. This may manifest itself in the form of interference on communication and sensor systems, cockpit display distortions, flight control problems and initiation of ordnance etc. As avionics systems become more reliant on high speed mission computers, failures of these types, particularly in safety critical systems, is becoming a serious concern in today's increasingly severe electromagnetic environment (EME). There is consequently a growing need to test aircraft, both military and commercial, for Electromagnetic Compatibility (EMC) between subsystems and within their operational EMEs.

Inter-system testing gauges the aircraft's electromagnetic compatibility with its defined external operational EME. The aim is to identify systems which, when exposed to the external EME, might prevent the aircraft from safely and effectively fulfilling its mission. For military applications the environments and guidance for inter-system testing is found in MIL-STD-464A and for civilian applications the relevant standard is SAE Standard ARP5583.

In earlier work, a reverberation chamber (RC) was built and tested at the Defence Science and Technology Organisation (DSTO) in South Australia for full level inter-system testing (also known as electromagnetic vulnerability (EMV) testing) and works well at frequencies >30 MHz. Because of fundamental limitations, the RC does not access the HF region (2 - 30 MHz) of the communication spectrum. DSTO has been conducting research into Transverse electromagnetic (TEM) Cells, which are test chambers that can generate plane wave electromagnetic field exposure for equipment under test in the HF frequency range. Typically TEM cells are used to test small items such as computers and other portable electronic devices. In this study the focus is on applying the method to whole aircraft EMV testing with the ultimate goal of combining a TEM cell with an RC to provide a hybrid testing facility capable of testing from 10 kHz to 18 GHz.

To investigate the applicability of the TEM cell technique to aircraft testing, computational electromagnetic (CEM) modelling has been used to investigate a scale TEM cell built on the DSTO site. The understanding gained was then used to address electric field uniformity issues seen in the TEM cell at frequencies above 17 MHz for the full sized cell. This so-called "transition region" from 17 MHz to 30 MHz is unfavourable for EMV testing due to large variations in electric field strength with frequency. These field variations are known to be due to cavity resonances within the cell. A novel method of active mode cancellation has been developed through CEM modelling together with physical measurements and was shown to reduce the primary cavity resonance by 20 dB. With the use of this technique and with selective stepping over some frequency points, the TEM cell proved to be a potential option for whole aircraft EMV testing.

Authors

Andrew J. Walters
Air Operations Division

Andrew Walters is a Research Scientist in the Airborne Mission Systems branch of the Air Operations Division where he conducts research in the area of Electromagnetic Vulnerability testing of whole aircraft. Prior to his work at DSTO Andrew obtained a B.Sc.(Hons) in Physics and a Ph.D. in Nuclear and Particle Physics from the Flinders University of South Australia.

Chris Leat
Air Operations Division

Holds a B.Sc.(Hons) in Physics and a PhD in computational electromagnetics from the University of Queensland.

Contents

Appendices

Chapter 1

Introduction

Avionics systems have the potential to suffer from undesirable behaviour when exposed to radio frequency (RF) energy. This may manifest itself in the form of interference on communication and sensor systems, cockpit display distortions, flight control problems and initiation of ordnance etc. As avionics systems become more reliant on high speed mission computers, failures of these types, particularly in safety critical systems, is becoming a serious concern in today's increasingly severe electromagnetic environment (EME) [1]. There is consequently a growing need to test aircraft, both military and commercial, for Electromagnetic Compatibility (EMC) within themselves and their operational EMEs. This is summed up in the general requirements found in MIL-STD-464A "Electromagnetic Environmental Effects, Requirements for Systems". It states that:

"*The system shall be electromagnetically compatible among all subsystems and equipment within the system and with environments caused by electromagnetic effects external to the system. Verification shall be accomplished as specified herein on production representative systems. Safety critical functions shall be verified to be electromagnetically compatible within the system and with external environments prior to use in those environments. Verification shall address all life cycle aspects of the system, including (as applicable) normal in-service operation, checkout, storage, transportation, handling, packaging, loading, unloading, launch, and the normal operating procedures associated with each aspect.*"

Box level testing is conducted before the equipment is installed into the aircraft. The equipment must conform to standard emission and susceptibility levels documented in MIL-STD-461E for military applications and DO-160E for civilian. This testing is performed typically in a shielded semi-anechoic room by accredited EMC test houses. The EMC/EMI characteristics of a box forms the basis of analysis at the system level once installed in the aircraft.

The intra-system testing attempts to discover any RF interference between avionics boxes. This involves conducting a source-victim test procedure within the aircraft, whereby the performance of one system (victim) is monitored while other systems (source) are operated. If identified, the interference encountered can be due to currents conducted along adjoining cables or radiated emissions coupling to external antennas.

Inter-system assessment gauges the aircraft's electromagnetic compatibility with its defined external operational EME. The aim is to identify systems which when exposed to the external EME, will prevent the aircraft from fulfilling its operational requirements.

For military applications the environments and guidance for intra-system and inter-system testing is found in MIL-STD-464A and for civilian SAE Standard ARP5583. Our focus in this report is mainly on inter-system assessments of military aircraft. The types of inter-system assessment techniques which can be conducted depends upon the frequency range and the equipment available. At a top level they are grouped into Low-Level and Full-Level measurements.

The low level measurements focus on determining the transfer functions between the external EME and either the currents on cable bundles within the aircraft or the internal fuselage EME. Specifically:

- Low Level Direct Current Injection (LLDCI) can be used from 10 kHz to the first airframe resonance. It involves first computationally modelling the expected aircraft skin current characteristics for a standard plane wave exposure. These currents are then replicated on the physical aircraft by directly injecting a signal onto the skin of the aircraft (either at the nose or wing tips). The aircraft is typically positioned over a circular ground plane on an Open Area Test Site (OATS). Currents induced on the cable bundles within the fuselage are measured to determine the transfer function which is used to determine the likely cable currents for a particular external EME. This method is used where coupling levels are too low to measure with LLSC.

- Low Level Swept Current (LLSC) is typically used for frequencies up to 400 MHz, involves the aircraft being exposed to fields generated by a series of antennas on an OATS. Field levels generated at the aircraft are typically no more than 1 V/m. Cable bundle currents are once again measured to determine the transfer function relative to an external EME.

- Low Level Swept Field (LLSF). This measurement is applied for frequencies from 100 MHz to 18 GHz. It is used to determine the transfer function between the internal and external EMEs relative to the aircraft. In essence it is a measurement of the shielding effectiveness or RF attenuation of the fuselage. An aircraft can be exposed to low level fields on an OATS, in a reverberation chamber (RC) or anechoic chamber (AC) while the internal fields are measured. The results can be scaled to give the internal EME for a particular external field level.

These methods can be used to determine the environment, both conducted and radiated, within the aircraft for a particular external EME. The extrapolated environment levels are compared with the box level characteristics to identify any potential failures. Frequencies where the analysis indicates internal EME levels greater than the box level vulnerabilities may require a full level test. For military applications, it is typically accepted that full level testing is required at all 'driver' frequencies. Full level testing is also conducted with the aircraft on an OATS, in an AC or in a RC [2, 3]. The choices of full level testing are:

- Full Level Direct Current Injection (FLDCI) is a similar procedure to LLDCI with an injection level which corresponds to the full level of the external EME. This method is the subject of research at DSTO. The upper frequency would need to exceed the first airframe resonance for this method to be practical.

- Bulk Current Injection (BCI) is typically applied for frequencies below 400 MHz. Current clamps are used to inject full EME level currents onto selected cable bundles within the aircraft's fuselage. The location of the aircraft is irrelevant as radiation is negligible.
- Full Level Field (FLF) is typically used from 100 MHz upward [2]. The aircraft is exposed to the full external EME field levels while monitoring the operation of its systems. This can be achieved on an OATS, in a RC or in an AC.

The inter-system EMI/EMC testing of an aircraft, military or commercial, can therefore be achieved by either low-level or full-level testing or a combination. One difficulty in the techniques arises from the use of an OATS. The OATS can be restricted in the frequency range available for testing due to spectrum licensing. Furthermore, the cable bundle measurement and injection techniques require a level of engineering judgement to be applied when determining which of the numerous bundles are chosen for investigation. Therefore the result may not be accurately representative of an aircraft exposed to an EME in free space. At frequencies above 30 MHz, testing can be more rapidly achieved by the use of an RC instead of the OATS. An RC is a shielded room into which RF energy is transmitted. A conductive stirrer is used to stir the standing waves created inside and so produce an isotropic randomly polarised EME for testing. An RC exposes the aircraft to EME level field levels in its entirety, without the need for multiple antenna positions and polarisations as is required on the OATS and in an AC. Its drawbacks include the loss of directional information if an aircraft failure is identified, large power requirements and minimum pulse length limitations. However, the ability to carry out tests swiftly, from more apparent antenna positions, outweighs the disadvantages to some extent.

A reverberation chamber (RC) was built and tested at the Defence Science and Technology Organisation (DSTO) in South Australia for full level inter-system testing (also known as electromagnetic vulnerability (EMV) testing) and works well at frequencies >30 MHz where mode density is sufficiently high. Unfortunately the RC does not access the HF region (2 - 30 MHz) of the communication spectrum. In order to conduct EMV testing in this HF frequency range, DSTO currently uses the OATS technique together with BCI to achieve full level testing. Our current research program is looking at an alternate testing method in the HF range which is free of the OATS limitations. TEM (Transverse Electromagnetic) cells traditionally used for box level testing at low frequencies could be the solution.

A TEM cell may be thought of as the expansion of a coaxial transmission line, whereby the outer-conductor of the coax is connected to a shielded cavity and the inner-conductor is connected to the end of a septum which is suspended the cavity. The other end of the septum, is terminated with a load. The space between the septum and outer cavity is made large enough to house a test object. At the feed and load points of the TEM cell, the structure has tapered ends to provide a gradual impedance matching from the coaxial transmission line. With a signal placed on the septum a single polarised travelling wave is produced representing a far field plane wave in free space. This normal TEM operation is possible for frequencies below that at which cavity resonances are seen. The advantage of the TEM cell over the OATS is that it provides a test environment isolated from external influences: continuous access to the RF spectrum within the cell's operating range; protection from weather factors on equipment; and the added security of a lockable

facility. The TEM cell design, otherwise know as the "Crawford style" [4], is not without its limitations. Confined test volume, frequency limits due to the appearance of higher order modes, and polarization restrictions are problems which have been the main motivation behind many of the TEM cell studies. Other methods of constructing TEM cells have been proposed and modelled in which improved performance has been obtained through changes in septum design and loading methods. For example, Carbonini [5] reports on a cell with double polarization and balanced wire septa, the X-TEM cell, resulting in optimization of the test volume dimensions.

In the literature, TEM cells have been proposed for whole vehicle testing either as a separate test facility [6, 7], or in a hybrid configuration with an RC [8, 9, 10]. The hybrid facility is an attractive option for the complete Electromagnetic Vulnerability (EMV) testing of military and commercial aircraft. A facility housing both test methods has the potential to test an aircraft's EMV for frequencies between 10 kHz and 18 GHz. The concept was first proposed and investigated by Crawford *et al.* [8]. A 1/10 scale model was constructed and used to determine the viability of the proposal for EMV testing. The basic design utilised a dual stirrer RC constructed with two orthogonal septa to provide horizontal and vertical polarisation in the TEM mode. Measurements were taken to assess the TEM and RC operation of the design. Three regions of operation were identified, TEM, stirred mode (reverberant) and a transition region in between the two which was neither TEM nor reverberant. In the transition region the uniformity of the test field is lost due to cavity resonances. These resonances break down the plane wave TEM operation, but are too widely spaced in order to provide adequate overmoded RC operation. Many attempts have been made at reducing the extent of the transition region [9] by operating the RC undermoded. Investigations into improved stirrer designs as well as the addition of RF absorption material are just a couple of the research thrusts. However, none have proved practical for a RC/TEM hybrid facility at this time.

A reduction in efficiency and field uniformity is also experienced when using the TEM component in a horizontally polarised mode due to the typical reverberation chamber being other than a cube. Crawford *et al* [8] also found that the TEM operation required 20 dB more power than the RC operation to achieve the same test EME levels. In summary, there are many challenges ahead to make the hybrid facility a reality but with many rewards if successful. This challenge forms the basis for the DSTO research program into TEM cells and a hybrid facility.

This report details the DSTO research to date on achieving a viable RC/TEM hybrid EMV testing facility for military aircraft. Chapter 2 documents the stages of research into characterising an asymmetric TEM cell. In particular: Section 2.1 describes the DSTO research TEM cell, Section 2.2 details the development and validation of a computational electromagnetic (CEM) model of the DSTO TEM cell, Section 2.3 shows investigations into the applicability of the DSTO TEM cell design to reproduce free space conditions for aircraft and Section 2.4 tackles extending the frequency range of TEM operation thereby reducing the transition region for a hybrid facility. Chapter 3 proposes the possible options for incorporating a TEM cell into the DSTO RC suggesting some possible designs and their associated costing.

Chapter 2

TEM Cell Research

2.1 The DSTO TEM Cell

2.1.1 Physical Cell

An asymmetric "Crawford style [4]" TEM cell exists at DSTO for research purposes. It was intended to be a scale model of what could be implemented in the existing reverberation chamber (RC) to form a hybrid system, and its proportions are so based. The DSTO reverberation chamber is shown in figure 2.1 and the TEM Cell in figure 2.2. The reverberation chambers dimensions are 29 m x 11 m x 6 m. The TEM cell is scaled down by a factor of 4.7 from its intended size inside the RC in order to fit inside a standard sized cargo container maintaining the same width and height ratio as the RC. The cargo container provided a convenient structure to secure the TEM cell to, as well as providing security and weather protection. For ease of access to the testing volume of the TEM cell, its orientation is rotated 90° to that intended in the full size version. Therefore the septum hangs vertically producing a horizontally polarised electric field, whereas the intention for an aircraft sized TEM cell is to have the septum placed horizontally in the upper third of the RC for a vertically polarised field.

The outer dimensions transverse to the propagation direction are 2.335 m by 1.27 m, and length of the parallel section is 2.26 m. The tapered sections are 1.114 m long and the feed points of the solid metal septum are offset 0.29 m from the cell wall (see figure 2.3). The asymmetry was employed in an attempt to maximise the test volume which, for a symmetrical TEM cell is generally accepted as 1/3 of the volume bounded by the septum and the outer. One end of the septum is connected to a signal source and the other end to a high power 50 Ω load.

2.1.2 CEM TEM Cell Model

The intention for this study was to use computational electromagnetics (CEM) to optimise a TEM cell design in order to reproduce the free space conditions a military aircraft would encounter in its normal area of operations. CEM can be used to calculate near fields,

Figure 2.1: *DSTO reverberation chamber containing the F/A-18 during the 2001/2002 ASRAAM trial.*

far fields, surface currents and an array of antenna parameters for a computer representation of a physical structure involved in an RF environment. A computer representation of the DSTO TEM cell, including the electrically-separate septum was constructed in the FEKO software package [11]. FEKO is a commercial electromagnetic software package capable of hybrid UTD/MoM operation. We used the Method of Moments (MoM) capability, which is based on the well known Rao-Wilton-Glisson basis functions.

The TEM cells dimensions were obtained from the original CAD design to construct the cell in FEKO using MoM parallelograms and triangles. The final structure was meshed with triangles for calculation, with a mesh density assigned by the FEKO package according to the intended frequency. If multiple frequencies were to be investigated, the highest frequency was used for the mesh density with 10 MHz added to ensure computational convergence. Narrow plates were used to connect each septum end to its adjacent outer shell region. This construction mimics the coaxial connectors at the ends, the shield of which is connected to the outer chamber, and the inner of which is connected to the septum tip. One septum end was then driven with a voltage source, and the other was loaded with a 50 Ω resistance. The model is shown in figure 2.4.

Figure 2.2: *DSTO TEM cell. Shown is the septum (top left), Side positioning (middle), Side access (top right) and the shipping container in which it is housed (bottom right).*

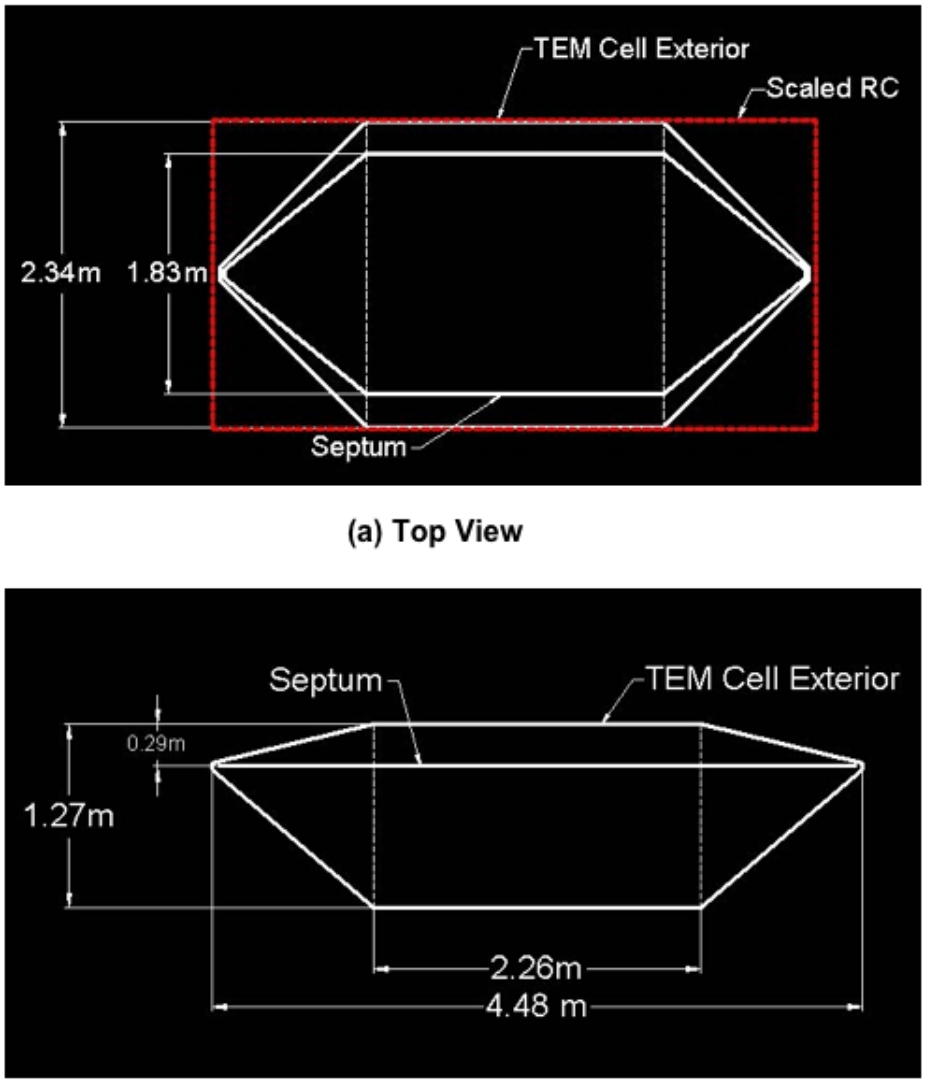

Figure 2.3: *DSTO TEM cell dimensions. The red rectangle in (a) shows how the full sized TEM cell would be incorporated inside the 21 m long DSTO RC.*

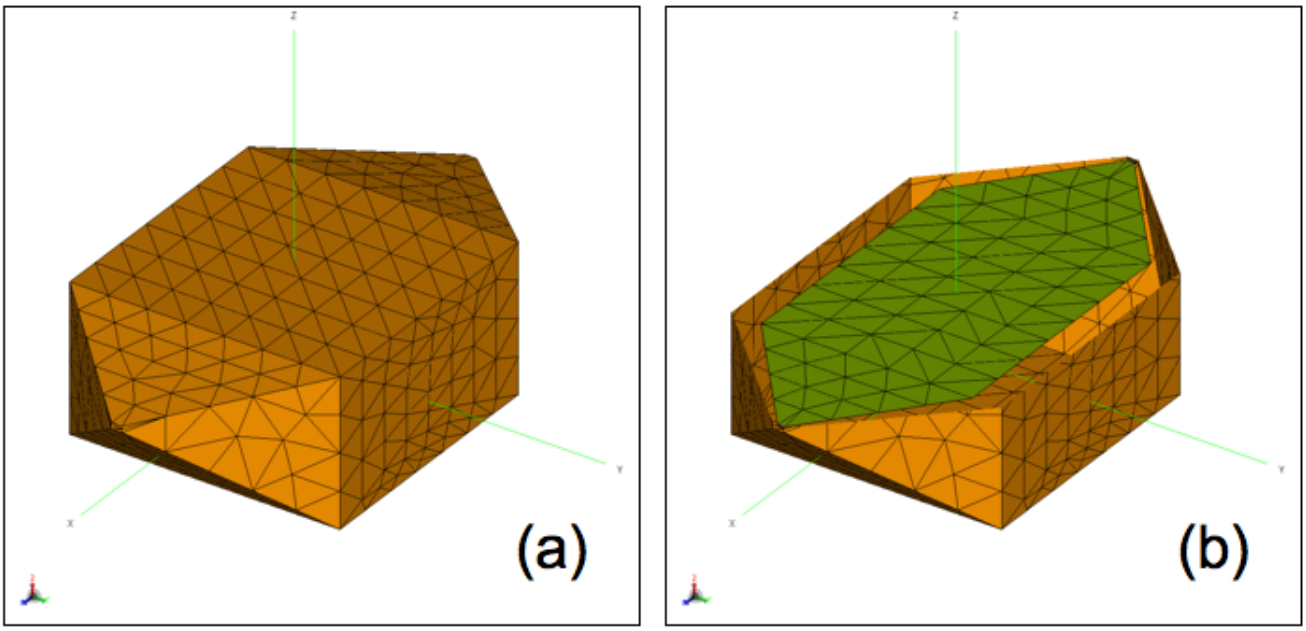

Figure 2.4: *FEKO model of the DSTO TEM cell. (a) shows the Method of Moments mesh on the TEM cell, (b) shows a cut-away view with the septum in green.*

2.2 CEM Model Validation

The major aim of our study is to investigate the potential for EMV testing a whole aircraft using a TEM cell. We intended to investigate this through various TEM cell designs initially through Computational Electromagnetic (CEM) modelling and then progress on to the measurement of a physical system once a promising design has been identified. The DSTO TEM cell provided a baseline design on which our modelling technique could be validated. To validate the TEM cell model described in section 2.1, electric field measurements were taken inside the physical cell and then compared with equivalent field points calculated from the CEM model. This section describes this validation process.

2.2.1 Measurements

The aim of the initial experiments performed on the physical TEM cell had two parts:

1. The first part of the experiment was to investigate the effect of an E-field probe's supporting structure on electric field measurements made inside the DSTO TEM Cell. This would therefore determine a possible preferred orientation of the probe's structure to minimise perturbation of the E-field during measurements.

2. The second aim of this experiment was to collect data which could be used to validate the CEM (computational electromagnetic) model of the TEM cell. The parameter to be compared with theory was electric field strengths inside the DSTO TEM cell.

The equipment used in the experiments is listed in table 2.1. The TEM cell was set-up in the standard manner. A high-power broadband 50 Ω load was connected to one end of the TEM cell septum, and the input power was coupled into the other end via a directional coupler so that forward and reverse powers could be recorded. An E-field probe served as the main measuring device and was mounted on a non-coducting stand to enable positioning at multiple points, see figure 2.5.

Table 2.1: *Equipment List*

EQUIPMENT TYPE	MODEL	FREQUENCY	SERIAL#	QTY
E-Field Probe	HI-4433-HSE	0.5 MHz to 1.5 GHz	S/N 85241	1
Power Amplifier	AR150A100	10 kHz to 100 MHz	–	1
Power Amplifier	AR100W100M1	80 MHz to 1.0 GHz	–	1
Power Meter	HP438A	–	S/N 3513U06103	2
Power Sensor	HP8482H	100 kHz to 4.2 GHz	S/N 3318A07092	
Directional Coupler	ARDC2600	10 kHz to 250 MHz	S/N 19729	1
50Ω Load	Model 8135		S/N 25606	1

2.2.1.1 E-Field Probe Orientation

To determine if there is a preferred orientation for the E-field probe, the E-field was measured in the TEM cell for various orientations of the E-field probe. The location for

Figure 2.5: *E-Field probe on a non-conducting stand in the TEM cell.*

the probe head is shown in figures 2.6 and 2.7 whereby it was positioned such that its coordinate system aligned with that of the cell. Note the orientation of the TEM cell coordinate system is indicated in figures 2.6 and 2.7.

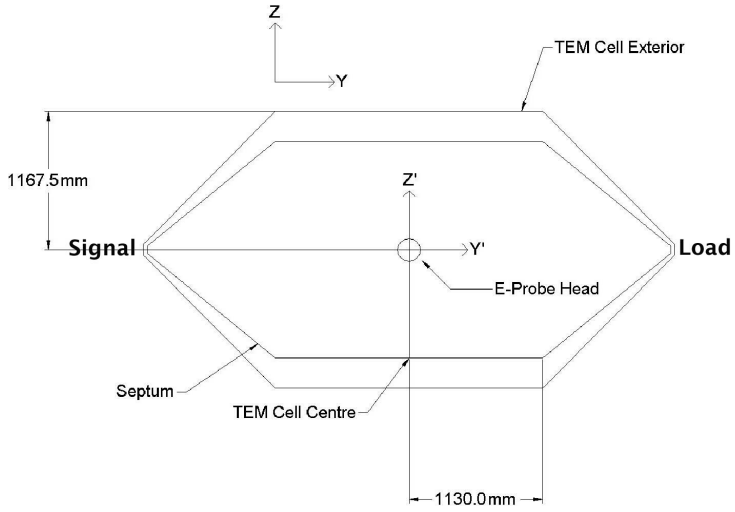

Figure 2.6: *Side view of the DSTO TEM cell. Shown is the probe head position 1, with orientation 1 (see table 2.2), for the E-field measurements.*

With the probe head aligned, E-field measurements were taken for different probe stem-housing positions. This was achieved by rotating the probe about one of the three axes at 90° intervals, resulting in the positions listed in table 2.2. In addition to these positions two more were carried out, positions 11 and 12, see table 2.2. These extra measurements were included to ensure coverage over the range of all possible orientations. For each of these positions the E-field was measured at 50 logarithmically-spaced frequency points from 0.5 MHz to 250 MHz, the results are shown in figure 2.8.

The results in figure 2.8 indicate that for all but one of the orientations, the electric field

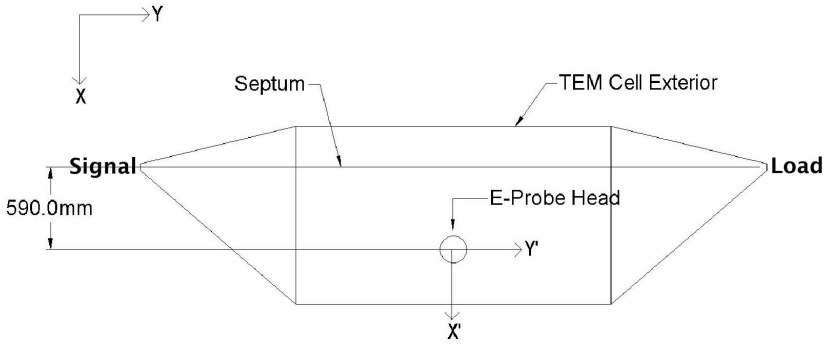

Figure 2.7: *Top view of the DSTO TEM cell. Shown is the probe head position 1, with orientation 1 (see table 2.2), for the E-field measurements.*

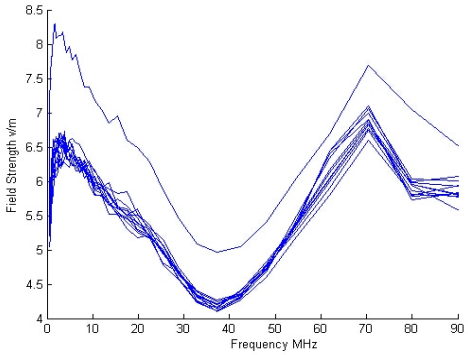

Figure 2.8: *Electric field strength measured for various E-field probe orientations as a function of frequency. A limited frequency range from that measured is plotted to highlight the separation between the curves.*

strength varied by less than 1 dB between probe axes positions. The curve for orientation-12 table 2.2, is not within the grouping of the other orientations but still only varies by less than 2 dB. This is expected, since orientation-12 is worst case with the electronics box at the end of the probe stem located within close proximity to the septum. Overall the probe orientation results indicate that the positioning of the probe stem is not critical to the electric field measurements inside the TEM cell.

2.2.1.2 Electric Field Mapping

With the influence from the probe stem eliminated, the aim was to measure the electric field of a plane within the TEM cell to validate the CEM model against. The probe head was positioned such that its axes, x′, y′ and z′, were lined up with the x, y, z axes of the TEM cell. With the probe in this orientation, the electric field was sampled at nine different positions in the TEM cell. These positions are shown in figures 2.9 and 2.10.

Table 2.2: *E-Field probe stem orientations. TEM cell axes are x,y,z. Probe axes are x', y', z'.*

TEM cell (probe orientation)	x	y	z
1	x′	y′	z′
2	x′	-z′	y′
3	x′	z′	-y′
4	x′	-y′	-z′
5	-z′	y′	x′
6	-x′	y′	-z′
7	z′	y′	-x′
8	-x′	-y′	z′
9	y′	-x′	z′
10	-y′	x′	z′
11	stem towards -y		
12	stem towards -x		

At each position the electric field strength was measured again at the 50 frequency steps. The symmetry made three of the probe positions redundant, although they provided a good check on the results. The probe axes were aligned with the cell axes during the measurement. Input powers to the TEM cell were chosen to produce electric field strengths within the operational range of the field probe.

For comparison with the CEM model, all measurement results were scaled to give peak electric field strength per root watt of input power. In the case of the measured data, the equation:

$$E_{peak,effective} = \frac{E_{peak,measured}}{\sqrt{P_f - P_r}} \tag{1}$$

was used. Where $E_{peak,measure}$ is the measured electric field strength in V/m, P_f is the forward power and P_r is the reverse power. The measured field strengths, normalized to 1 watt input power, are given in figure 2.11 for the lower frequencies, where the behaviour is predominantly TEM. Only six positions are shown for clarity, the other three being redundant due to symmetry. Fluctuations in field strength are seen between 4 $\mathrm{Vm^{-1}W^{-\frac{1}{2}}}$ and 7 $\mathrm{Vm^{-1}W^{-\frac{1}{2}}}$, indicating a standing wave(SWR) of 7/4=1.75.

2.2.2 CEM Model Calculations

The TEM cell, including the electrically-separate septum was meshed in FEKO where the calculations were performed. An arbitrary voltage of 1V RMS was then used to excite the numerical model. The construction of the model is described in more detail in Section 2.1. Similar to the measurement results, the CEM results were scaled to give peak electric field strength per root watt of input power. The data was scaled using the equation:

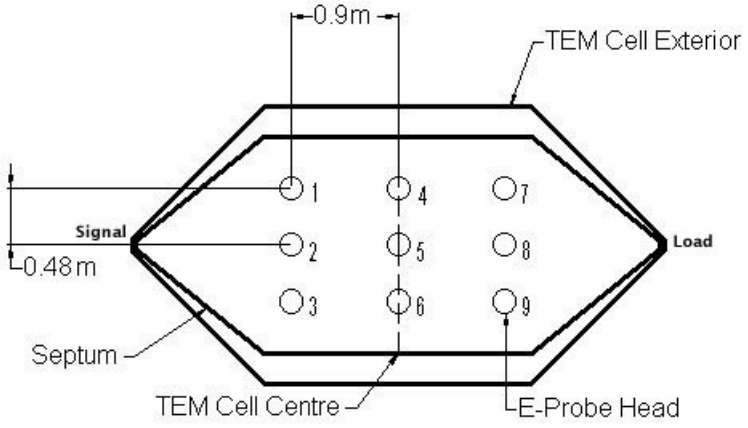

Figure 2.9: *Locations for field measurements in the TEM cell looking squarely at the septum.*

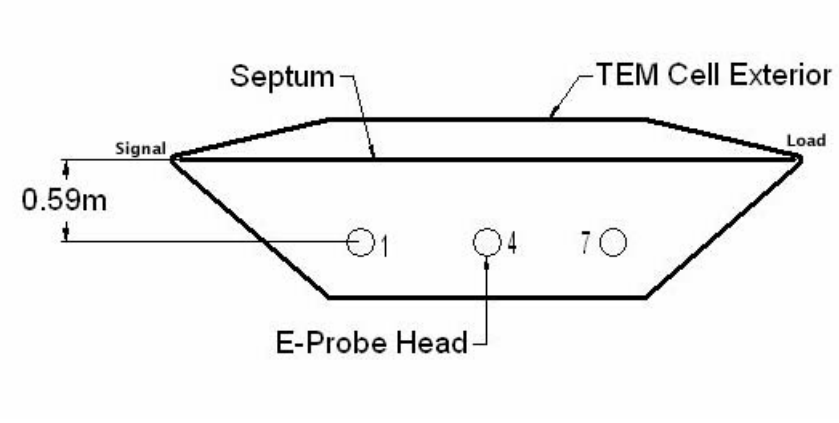

Figure 2.10: *Locations for field measurements in the TEM cell looking edge-on to the septum.*

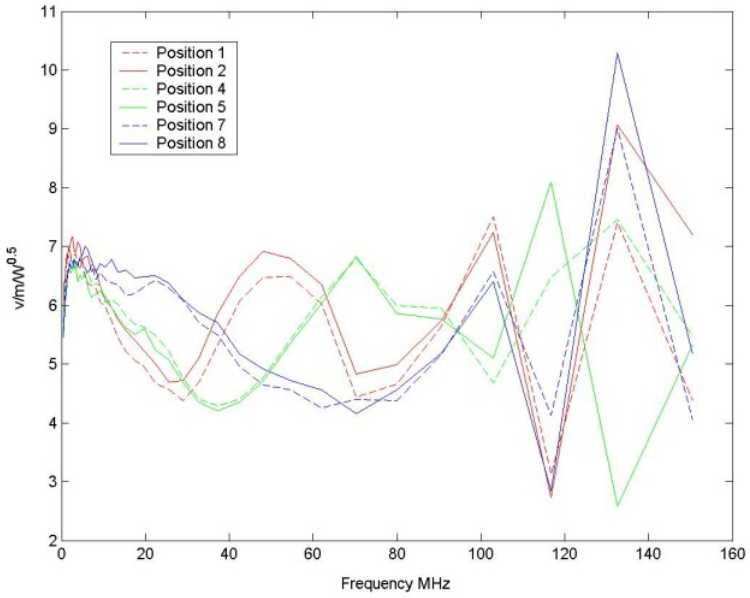

Figure 2.11: *Measured electric field strengths inside the TEM cell, normalized using equation (1).*

$$E_{peak,effective} = \frac{E_{peak,computed}}{\sqrt{\Re(\frac{1}{Z})}} \tag{2}$$

is used, where Z is the input impedance, $E_{peak,computed}$ and $\Re$ denotes the real part of the complex number.

Initially field slices were generated transverse to the septum, along the axis of the cell as shown in Figure 2.12, Figure 2.13, and Figure 2.14. A single instant in time is pictured. In the contour plots, hot colours represent more intense fields. Inside the cell, at low frequencies (Figure 2.12), the stronger fields between the septum and its nearest cell wall, and weaker fields in the test volume are consistent with the TEM modal operation. At 100 MHz (Figure 2.13), the propagating behaviour of the signal is evident in the three null surfaces, which can be seen marching from left to right when the phases of the source are used to generate the full cycle. At 200 MHz the behaviour in Figure 2.14 is seen, where a complex non-TEM mode is present and field uniformity is poor. In all three cases it is clear that fields exist outside the cell. These are not problematic as the levels are low (∼30 dB down) and the inevitable result of small numerical errors in the currents placed on the cell walls.

2.2.2.1 Model and Measurement Comparison

The initial results for the numerical model and the measurements are compared in Figure 2.15. Below 150 MHz both show TEM behaviour, with field levels of approximately 5 $\mathrm{Vm^{-1}W^{\frac{1}{2}}}$. At frequencies above about 150 MHz, higher order modes appear which give

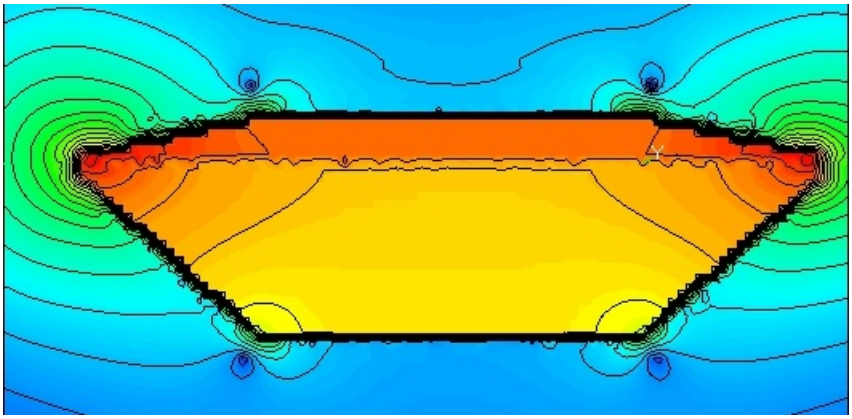

Figure 2.12: *Electric field contour plot at 1MHz.*

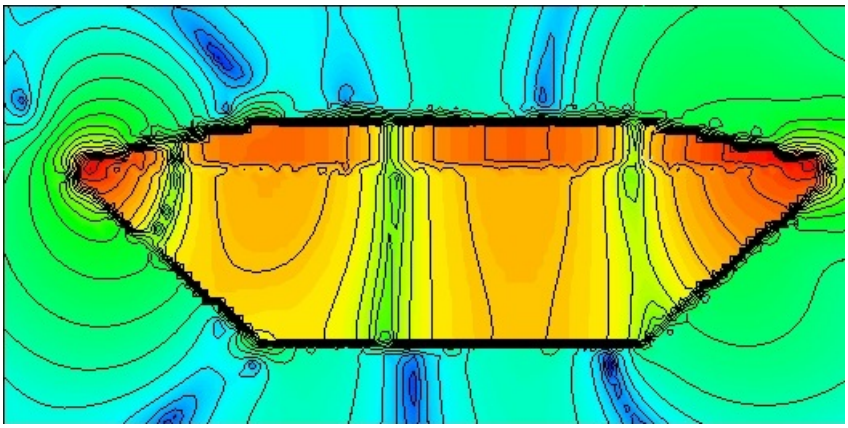

Figure 2.13: *Electric field contour plot at 100MHz.*

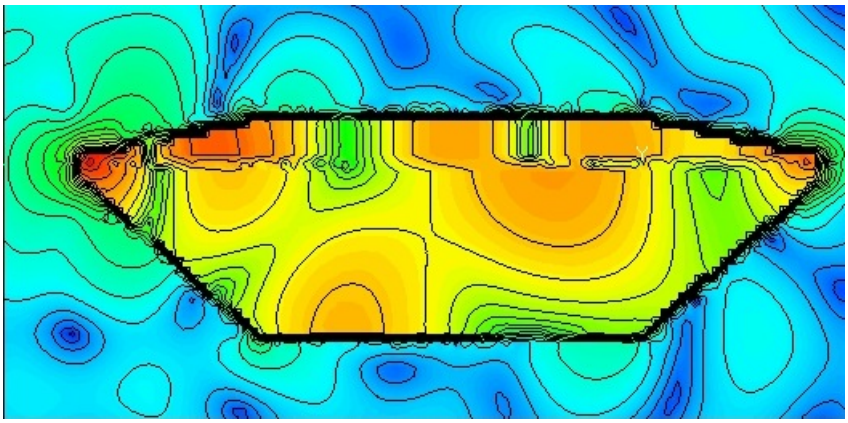

Figure 2.14: *Electric field contour plot at 200MHz.*

large increases in the fields for given input powers. This is a result of the inability of the coaxial load to damp the modes. These modes have poor field uniformity however, as shown in Figure 2.14. The comparison results in Figure 2.15 show a stark disagreement at 80 MHz. It was suggested at the time of the study that this may have been a TEM mode traveling side-to-side on the septum, since the septum width is $1/2\lambda$ at 80 MHz.

On repeating the measurements for a restricted range it was found that an equivalent resonance peak also existed in the measurements. The peak, at approximately 80 MHz is the TE_{011} mode. The measured and modeled peaks differed slightly in frequency, and the relatively coarse sampling initially used, had missed the very narrow band peak in the measurements. A much finer sampling was adopted with a 100 kHz step for both measurement and modeling, and the results are displayed in figure 2.16. The figure shows total electric field generated at a central point in the TEM cell for 1 W of nett input power.

The desired TEM mode is present below 79.8 MHz and between the peaks at 79.8 MHz and 123 MHz. It is seen that the measurements and model agree very well upon the level of field for the TEM mode with a discrepancy of less than 2 dB. Above the 123 MHz peak, it is not apparent what the relative contributions are from TEM and resonant modes. Total field levels agree well, however. It is clear that all the resonances present in the model are present in the measurements with some disagreement in frequency by approximately 2.5 MHz.

Some resonant peaks are seen in the measurements below 79.8 MHz, which disagrees with the theoretical minimum frequency for resonance in a cavity of this size, and with the numerical model. These peaks are due to the use of the E field probe together with third harmonic distortion in the amplifier. For example, the amplifier when excited at 41 MHz, is also producing some 123 MHz in its output. The 123 MHz signal excites the 123 MHz cavity resonance which is detected by the E field probe as part of the total field, with the result that it appears, incorrectly, at 41 MHz.

2.2.3 Validation Experiment Conclusions

In this study a computational electromagnetics model of the DSTO TEM cell was validated using measurement results. In addition the importance of using the two techniques in tandem to acquire a more accurate picture of the system was shown. Considering the empty TEM cell results scaled up to the RC dimensions, TEM behaviour is seen in the region below 17 MHz and also between 17 MHz and 26 MHz.

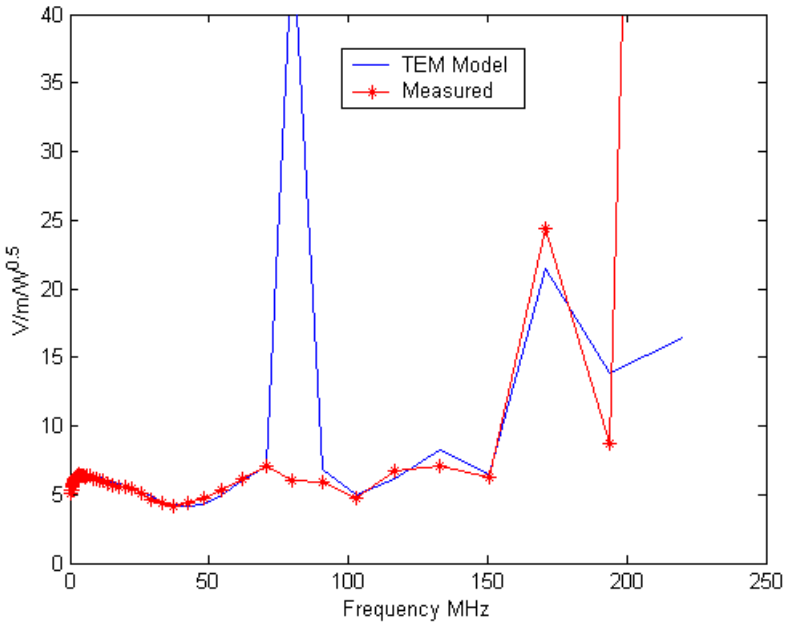

Figure 2.15: *Electric field comparison between the measured data and the modeled data.*

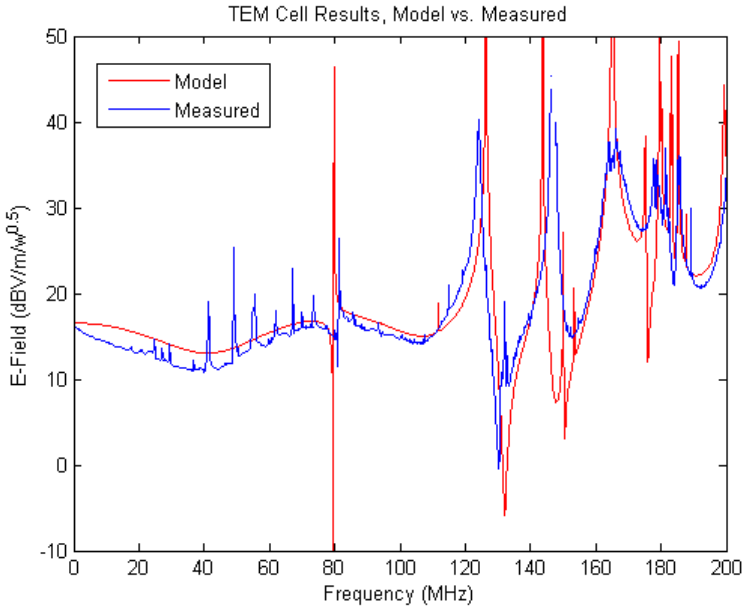

Figure 2.16: *Comparison between measurement and model results for the DSTO TEM cell with reduced sampling steps of 100 kHz.*

2.3 TEM Cell, OATS and Free Space Comparison

If scaled up for whole aircraft testing, how would the DSTO TEM cell compare to the current Open Area Test Site technique (OATS)? More specifically, when attempting to recreate the EME an aircraft would experience during flight (Free Space), which technique is more accurate? The investigations into which of the two techniques produce an EME closer to the Free Space case are described in this section. Hence forth the TEM cell model dimensions have been scaled up by a factor of 4.7 to represent the intended size of the cell for whole aircraft testing. Therefore the TE_{011} resonance at 79.8 MHz mentioned in Section 2.2 occurs at 79.8/4.7 = 16.98 MHz in the scaled-up cell. All the work in this section was based on computational modelling.

2.3.1 FEKO Models

The Macchi aircraft was acquired in 1967 for use with the Royal Australian Air Force (RAAF) and Royal Australian Navy (RAN), where it served as mainly a trainer aircraft. Now out of service, a Macchi has been obtained by DSTO for its EMC research program. We have therefore used it as the test subject to assess and develop the applicability of whole vehicle EMC testing in a TEM cell.

Three different cases were considered in our computational model investigations of the EMV test methods:

- A Macchi in Free Space for baseline purposes
- A Macchi on the OATS to test existing techniques
- A Macchi in the vertically polarised DSTO TEM cell.

The three method of moments (MoM) models are shown in Figures 2.17, 2.18 and 2.19 respectively.

The Macchi was meshed in an engineering modeling tool, FEMAP, from a CAD file and then entered into FEKO. FEKO [11] is a commercial electromagnetic software package capable of hybrid UTD/MoM operation. We used the MoM capability. The TEM cell and OATS ground plane were both constructed in FEKO from triangular surface elements. In the free-space and OATS environments, a standard FEKO plane wave source was used. For the TEM cell, the same construction was used as described in Section 2.1.2.

In Free Space and for the OATS model, a plane wave source was used and set to have a magnitude of 1 V/m. The driving voltage required to reproduce this environment in the TEM cell was calculated by finding the average field strength for a volume inside the empty cell at 10 MHz. Using this average field, the driving voltage was scaled up to produce an average field strength of 1 V/m. This voltage was found to be 4.6 V. For the OATS the electric field was calculated 2 m above the centre of the ground plane for frequencies 1MHz to 36 MHz at 1 MHz steps. These values were used as scaling factors at the various frequencies for the results obtained when the Macchi was present. This reflects normal OATS calibration practice in the field.

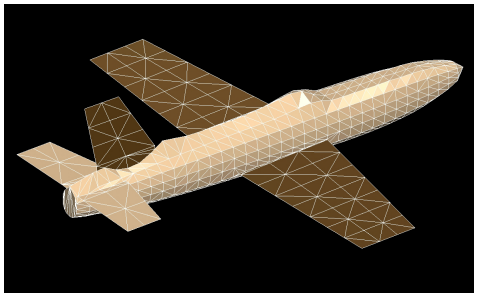

Figure 2.17: *Model of the Macchi aircraft in free space.*

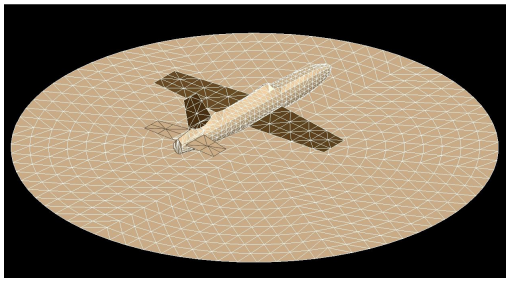

Figure 2.18: *Model of the Macchi aircraft on an OATS.*

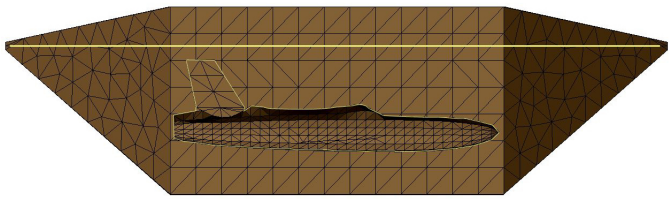

Figure 2.19: *Model of the Macchi aircraft in the DSTO TEM cell.*

2.3.2 Electric Field Intensification

The TEM cell design calls generally for minimum size due to the need to keep resonance frequencies high, and to reduce required input power levels. Additionally, in DSTO's case, a desire exists to modify the existing RC to create a hybrid design. Thus DSTO is pushing the limits of useable TEM cell volume, as a typical jet fighter occupies a considerably greater fraction of the TEM cell volume than is generally felt to be ideal. What could the effects be of the proximity of the aircraft appendages to the TEM cell walls? An obvious possibility is the intensification of electric field strengths in these areas, as charge accumulation on aircraft appendages leads to induction of opposite charges on the TEM cell surfaces and vice versa. Note that it is of no use to compare the fields around the aircraft to 1V/m, as we are considering the total field, not the incident field. Even in free space intensification of field strengths will occur near terminal points of the airframe. Near electric field strength is the determining factor in coupling to projecting conductors including monopole antennas, hence it is important the test method produces realistic levels.

To investigate the electric field intensification in the TEM cell and OATS compared to

free space, a series of field observation points were located 20 cm from key points on the Macchi aircraft (see Figure 2.20). As well as the eight shown, there is also one observation point directly below the cockpit which is not shown in the Figure.

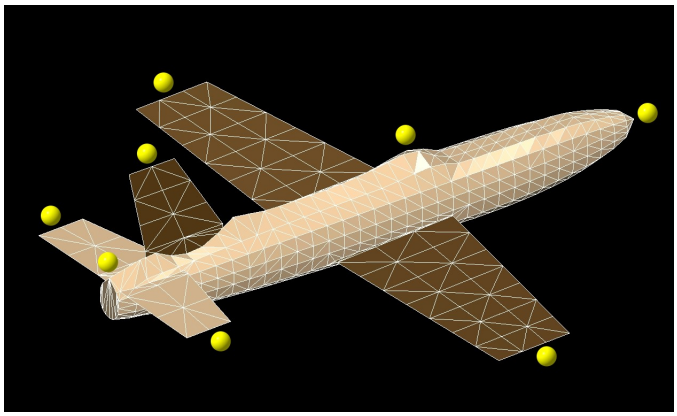

Figure 2.20: *Electric field observation points around the Macchi.*

For the Macchi in the TEM cell and in free space, the electric field strength at each of the nine points is calculated for frequencies 1MHz to 36 MHz at 1 MHz steps[1]. To maximise separations of the Macchi from the TEM cell walls, the cell was rotated 45° in the xy plane with respect to the Macchi's centre. This requires the plane wave sources in the OATS and free space cases to be at 45 degrees to the Macchi also.

The TEM cell, with the septum oriented horizontally above the Macchi, produces a vertically polarised electric field. The plane wave sources, for Free Space and OATS, were therefore given a vertical polarisation also in order to match the TEM cell configuration. The electric field strength was calculated at the designated points for the Macchi aircraft in the three environments. Electric field strength intensification was computed by dividing both the TEM cell and OATS fields magnitudes by the Free Space magnitudes. These ratios are plotted on a dB scale in Figures 2.21, 2.22 and 2.23 and identified as 'E-Field intensification'. Each subplot in the two Figures relates to a separate field observation point. The relative near electric field strengths plotted in Figures 2.21, 2.22and 2.23 provide a measure of the particular techniques ability to reproduce the Free Space electric field conditions seen by the Macchi aircraft. 0 dB is the ideal.

The field intensification results show a wide range of performance by the two testing methods. The OATS shows little field strength deviation from the free space results, $\pm$ 5 dB, for the wings, horizontal and vertical stabilizers. The fuselage and cockpit results show a slightly higher variation under testing almost down to -10 dB. There is however in all cases but one, increased field intensification seen around 12 MHz corresponding to the higher Q of the natural resonance of the Macchi airframe when against the ground plane. For the 'above cockpit' observation point only a small variation is seen at 12 MHz unlike the other points.

The first factor seen in all the TEM cell results is field intensification of up to 40 dB caused by the natural resonances of the TEM cell cavity. In order to negate this effect a

[1]Since the RC works down to 30 MHz, 36 MHz was chosen as the upper frequency to provide some overlap.

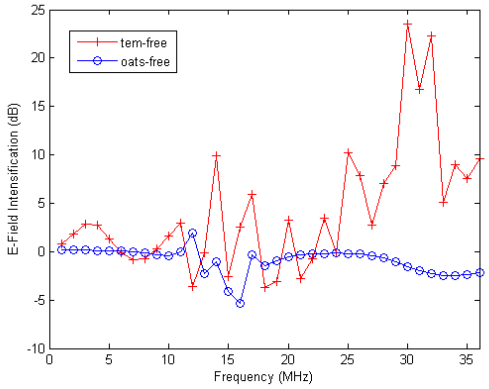

(1) Left Wing

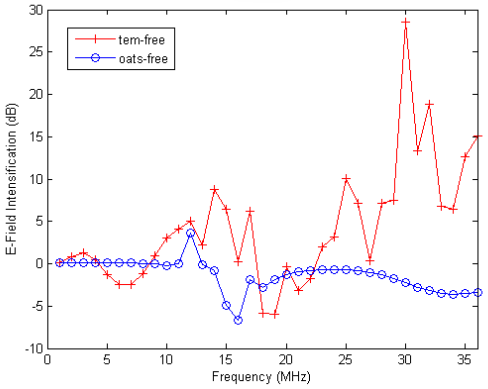

(2) Right Wing

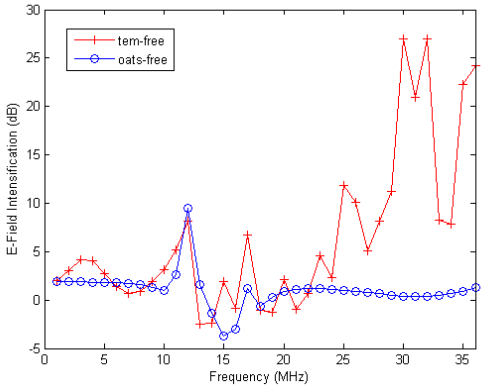

(3) Nose

Figure 2.21: *Electric field intensification relative to the free space case for the Macchi in the TEM cell and on the OATS.*

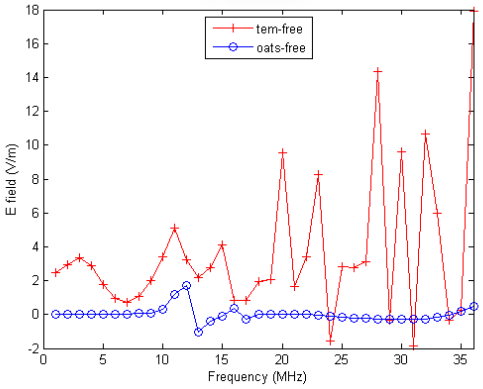

(1) Vertical Stabilizer

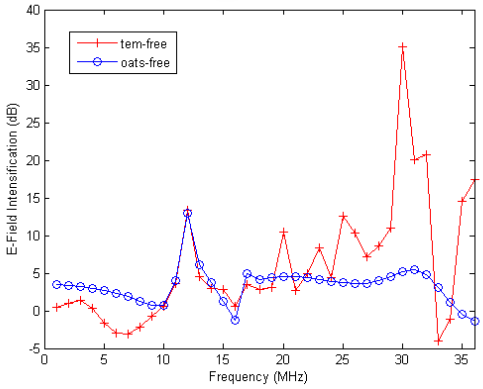

(2) End of Fuselage

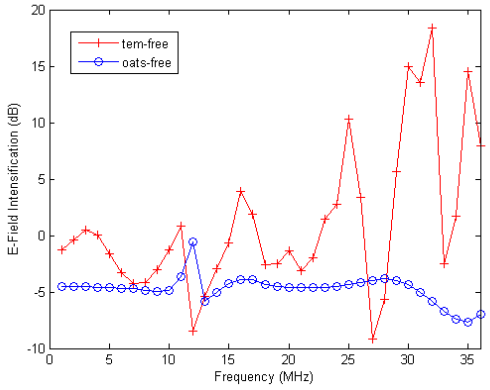

(3) Below Cockpit

Figure 2.22: *Electric field intensification relative to the free space case for the Macchi in the TEM cell and on the OATS. Cont ...*

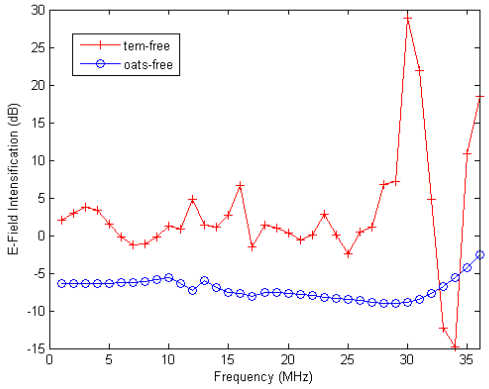

(1) Above Cockpit

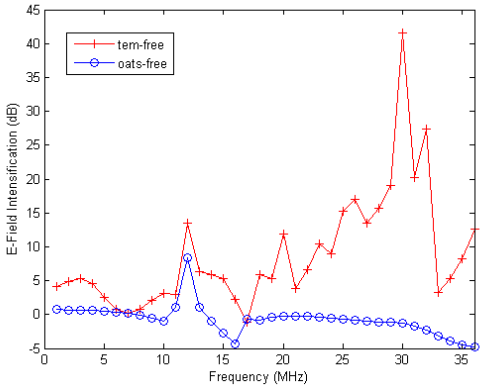

(2) Left Stabilizer

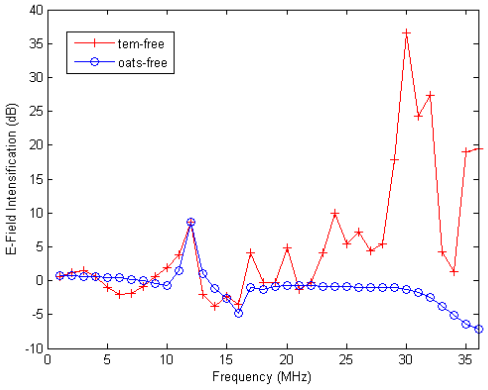

(3) Right Stabilizer

Figure 2.23: *Electric field intensification relative to the free space case for the Macchi in the TEM cell and on the OATS. Cont ...*

process of active resonance cancellation could be implemented. Experiments into active cancellation applied to the DSTO TEM cell are described in detail in Section 2.4.

Like the OATS, the Macchi airframe 12 MHz resonance is also seen is some of the TEM cell results. At frequencies away from the resonances of the TEM cell, the results are within ± 10 dB of free space and are comparable with the OATS. As mentioned earlier, appendage proximity to the TEM cell walls and septum may cause additional field intensity. Field intensification caused by the close proximity of appendages to the TEM cell walls could be reduced by increasing the dimensions of the cell relative to the aircraft. However, this would have the effect of shifting cavity resonances down in frequency and so reduce the frequency range over which pure TEM operation provides a uniform test field environment. It is clear that from an electric near field analysis, a mixture of an optimised geometry and active cancellation is the key to designing a TEM cell which can out perform the current OATS.

The analysis up until now has focused on field intensification. Besides this aspect there is also the potential of frequency shifts in the aircraft's natural resonance behaviour due to the presence of a ground plane or cavity walls. A shift of this type could be significant in a testing scenario where a particular resonance couples into an aircraft susceptibility. This would then indicate a possible weakness of the testing method's ability to reproduce free space conditions. Therefore the electric field strength calculated for the three Macchi situations (free space, OATS and TEM cell) are plotted in figure 2.24 for the right stabiliser only as an example. The comparison in figure 2.24 again shows the high Q nature of the aircraft resonance at 12 MHz when a ground plane is present compared with the free space case. However, there is no evidence of any considerable frequency shift between the free space instance of the resonance and that present in the TEM cell and OATS cases.

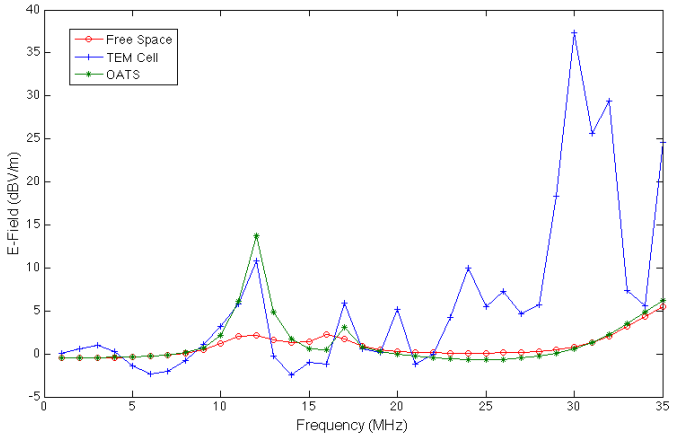

Figure 2.24: *Electric Field strength calculated at the right stabiliser observation point in the three cases: free space, OATS and TEM cell.*

2.3.3 Surface Current Investigation

The other and potentially more important component of producing a test environment is the skin currents on the test object induced by the incident electromagnetic fields.

Table 2.3: *Plane wave source configurations used for free space and OATS.*

Direction ϕ	Polarisation η
(Degrees)	(Degrees)
0	0
45	0
0	90
90	90

It is these surface currents which subsequently induce currents on the cables inside the aircraft's skin which in turn creates undesirable behaviour within the aircraft's avionics systems. In order to thoroughly test the applicability of the TEM cell methodology to EMV testing, we therefore studied the surface currents induced on the Macchi airframe through computation.

The aim was to gauge the ability of the TEM cell and OATS techniques to reproduce the frequency dependant surface current distribution of the Macchi aircraft for Free Space. The MoM method of calculation provides the surface current for each triangle within the surface mesh of the computational model. The meshed Macchi model contains 1739 individual triangles, each having a computed current characteristic. To minimise the volume of data used for comparison, a select number of surface mesh triangles were chosen as current observation sites. Sites were chosen to relate to the field observation points described in the last section. One site was chosen on each wing, nose, cockpit, horizontal and vertical stabilizers. Their positions are shown in Figures 2.25 and 2.26.

Surface currents were calculated using FEKO for frequencies between 1 MHz and 36 MHz at 1 MHz intervals. To obtain a more complete baseline for comparison, a range of source directions and polarisations relative to the Macchi aircraft were used for the OATS and free space calculations. The plane wave source orientations and directions used are listed in Table 2.3 and shown in Figure 2.27. Note that $\theta = 90^\circ$ for all cases.

A set of surface current results were obtained for each source orientation at frequencies 1MHz to 36 MHz in 1 MHz steps. For a particular case, Free Space or OATS, the maximum current density is calculated at each frequency point over all polarisations and directions using the following expressions:

$$J^{(n)}_{\substack{\text{free space}\\ \max}}(f) = \max_{i=1,4} |J^{(i,n)}_{\text{free space}}(f)| \tag{3}$$

$$J^{(n)}_{\substack{\text{OATS}\\ \max}}(f) = \max_{i=1,4} |J^{(i,n)}_{\text{OATS}}(f)| \tag{4}$$

where J is the current density in A/m, i represents the four different polarisation/direction configurations of the source (see Table 2.3), f is frequency, and n=1 to 7 corresponds to the 7 observation sites (Figures 2.25 and 2.26). The results for the 7 observation triangles are used to calculate the current intensification relative to the Free Space Macchi surface currents using equations 5 and 6.

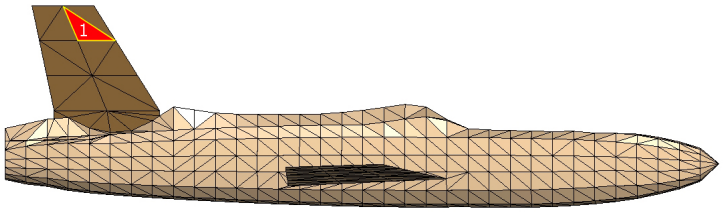

Figure 2.25: *The Macchi MoM model showing current observation triangle 1.*

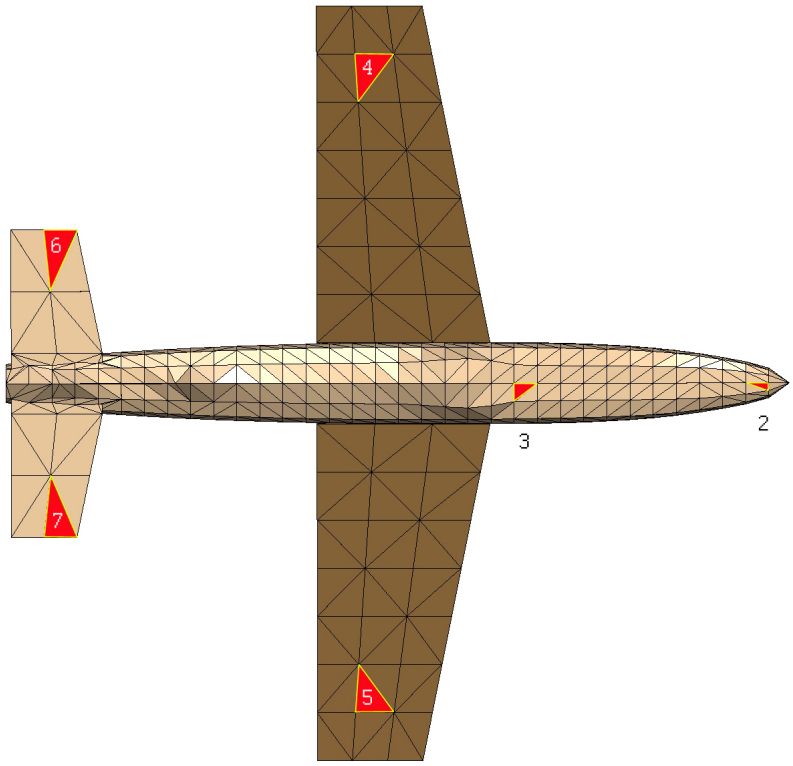

Figure 2.26: *The Macchi MoM model showing current observation triangles 2-7.*

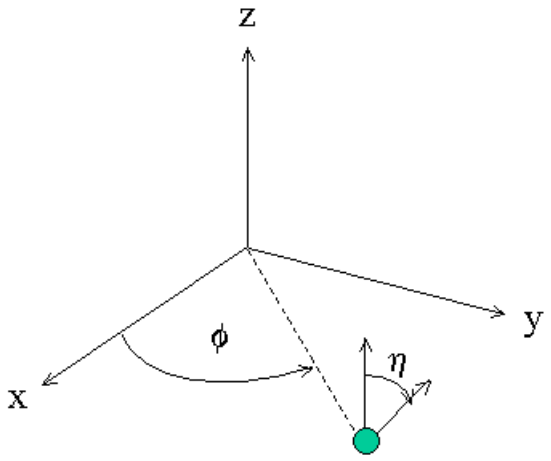

Figure 2.27: *Orientation of the FEKO plane wave source. ϕ represents the position of the source with respect to the x-axis in the x-y plane. η represents the polarisation of the source. Note that the Macchi aircraft is positioned with it's fuselage running along the x-axis.*

$$J^{(n)}_{TEM/Free}(f) = 20\log_{10}\frac{|J^{(n)}_{\text{TEM}}(f)|}{|J^{(n)}_{\substack{\text{free space}\\ \text{max}}}(f)|} \tag{5}$$

$$J^{(n)}_{OATS/Free}(f) = 20\log_{10}\frac{|J^{(n)}_{\substack{\text{OATS}\\ \text{max}}}(f)|}{|J^{(n)}_{\substack{\text{free space}\\ \text{max}}}(f)|} \tag{6}$$

where the current intensification is given in dB. This produced a curve for the OATS and for Free Space for each location 'n'. The TEM cell and OATS surface current results were divided by the free space currents, providing a relative comparison. The results are plotted in Figures 2.28 and 2.29. The ability of the test method to reproduce the surface currents seen on the Macchi aircraft in Free Space is gauged by the data's proximity to the 0 dB line in the plot.

In the subplots of Figures 2.28 and 2.29 three curves are plotted, 'TEM-Free Space' for $\phi = 45°$ and $\phi = 0°$[2] and 'OATS-Free Space'. Over all seven subplots there is a great degree of difference between the TEM cell results and the OATS results.

In general the TEM cell results exhibit lower surface current for frequencies below 27 MHz, getting as low as -30 dB in some cases. This is to be expected as the TEM cell does not reproduce horizontal E fields, which are known to couple to the airframe. Above 27 MHz the results generally show the opposite tendancy corresponding to the area containing the natural resonances of the TEM cell. For $\phi = 45°$, the TEM results show

[2]Unlike the E-field intensification work, the Macchi was positioned in two orientations inside the TEM cell. The possibility of an ideal aircraft position were investigated in this way.

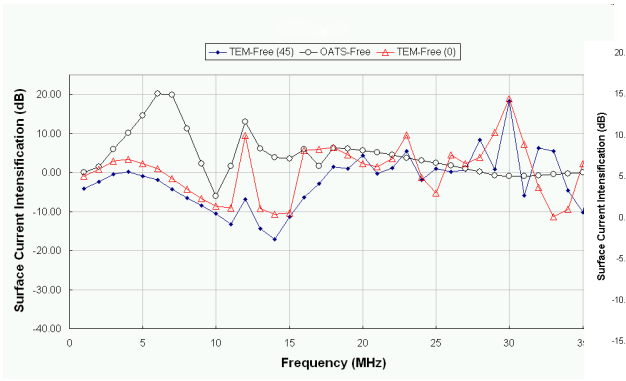

(1) Observation Site 1. Vertical Stabilizer

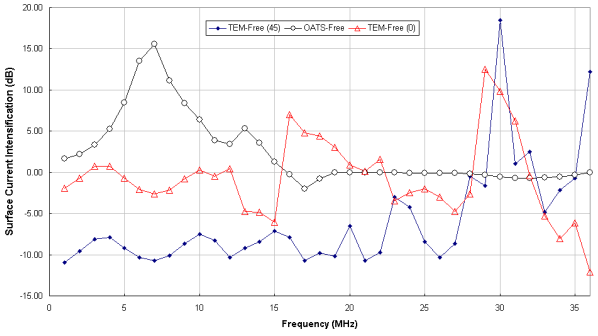

(2) Observation Site 2. Nose

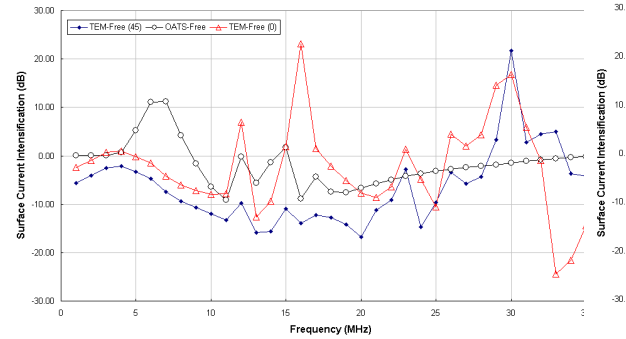

(3) Observation Site 3. Cockpit

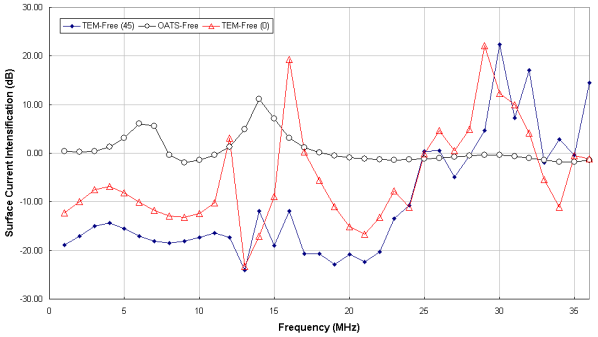

(4) Observation Site 4. Left Wing

Figure 2.28: *Surface current intensification* $J^{(n)}_{TEM/Free}(f)$ *for TEM+Macchi (0° and 45° orientation) and* $J^{(n)}_{OATS/Free}(f)$ *for OATS+Macchi.*

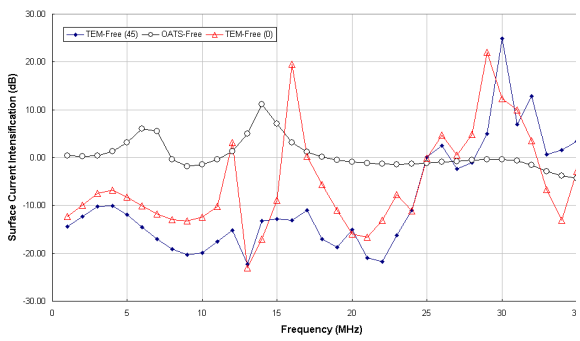

(1) Observation Site 5. Right Wing

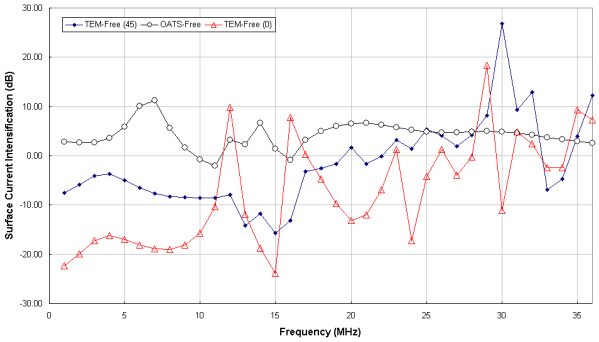

(2) Observation Site 6. Left Stabilizer

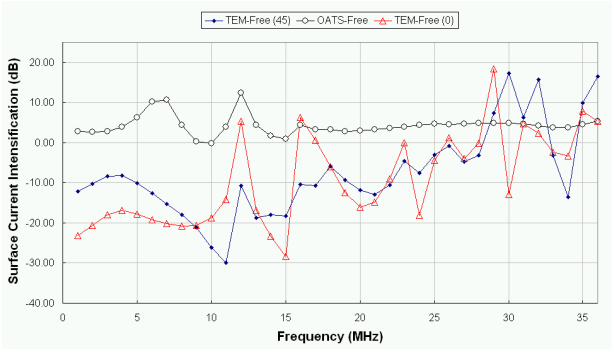

(3) Observation Site 7. Right stabilizer

Figure 2.29: *Surface current intensification* $J^{(n)}_{TEM/Free}(f)$ *for TEM+Macchi (0° and 45° orientation) and* $J^{(n)}_{OATS/Free}(f)$ *for OATS+Macchi. Cont ...*

less variation than for $\phi = 0°$ results. This is likely due to the greater distance between aircraft appendages and the cell walls for the 45° case. In $\phi = 0°$ results there are two resonances at 12 MHz and 17 MHz which cause current intensification over a narrow band of frequencies in each case. These are due to the airframe resonance in a high Q cavity and TEM cell TE_{011} mode respectively.This local intensification is seen to a lesser degree in the $\phi = 45°$ results due to a slight frequency shift for the different aircraft position and the relatively coarse sample steps.

For the OATS case all observation sites show an over test from 5 to 20 dB in the range of 5 to 7 MHz (Figure 2.28 and 2.29). It is likely that this is due to the ground plane causing a high curl component of the horizontal electric field. this results in a excessive magnetic field component in the propagation direction, which excites circulating currents on the airframe. On the infinite ground, this effect would become worse at lower frequencies. However the finite ground plane used here becomes electrically small below 5 MHz. Above 15 MHz the OATS results perform closer to the 0 dB line, with deviations up to 5 dB. Overall the OATS results have an above 0 dB trend for each of the observation sites and has better reproduction of the Free Space Macchi current profile than the TEM Cell. In addition the OATS shows less variation with frequency than the TEM cell which suffers at high frequencies from high order cavity resonances. However for both the TEM cell and OATS techniques, improvements could be made by adapting the input powers as a function of frequency to allow for the deviations from the Free Space case. This power adaptation is limited however, if there is considerable variation in amplitude between the observation sites within a technique.

Consider the Macchi in the TEM cell and on the OATS. At each frequency f we take the average of the respective surface currents. These averages then represent a factor which can be applied to scale the input power levels closer to the Free Space conditions (i.e. the 0 dB point on the y-axis of the intensification plots). The scaled results were obtained using the following expressions:

$$J^{(m)}_{\substack{TEM/Free\\Scaled}}(f) = J^{(m)}_{TEM/Free}(f) - \frac{\sum_{n=1}^{N} J^{(n)}_{TEM/Free}(f)}{N} \tag{7}$$

$$J^{(m)}_{\substack{OATS/Free\\Scaled}}(f) = J^{(m)}_{OATS/Free}(f) - \frac{\sum_{n=1}^{N} J^{(n)}_{OATS/Free}(f)}{N} \tag{8}$$

where $m = 1$ to 7 represents the observation sites, N=7 is the total number of observing sites and the current intensifications, J, are all in dB. It must be noted that this procedure cannot, however, diminish the spread in relative current levels between the 7 observation triangles. Figure 2.30 shows for the TEM cell, the current intensification curves for all 7 observation triangles after they have been adjusted in this manner.

The results in Figure 2.30 show that once adjusted the TEM+Macchi current intensification curves span approximately from -10 dB to +10 dB. The limiting factor for the procedure then becomes the current variation between observation sites across the Macchi

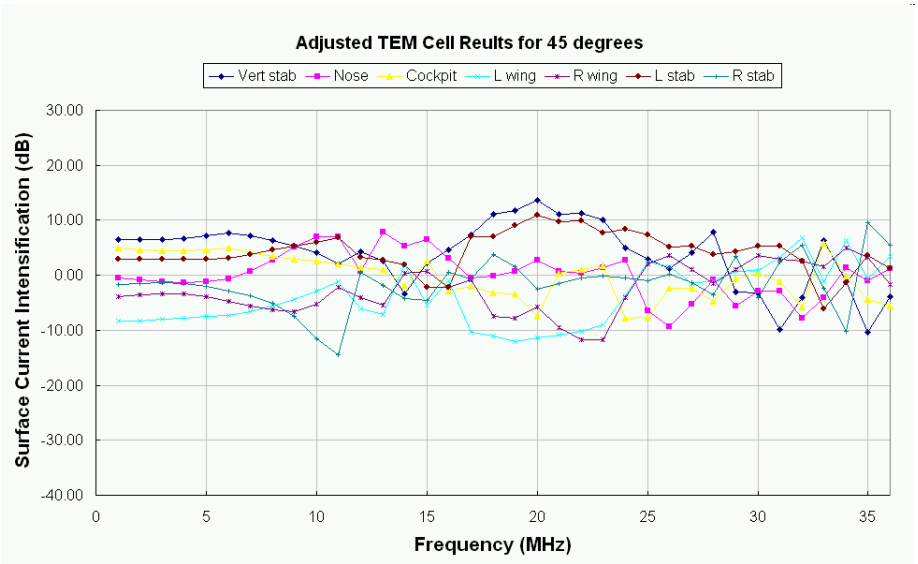

Figure 2.30: *Adjusted TEM+Macci surface current intensification curves for all 7 observation triangles. This is for the 45 degree TEM-Macchi orientation.*

aircraft. The large degree of variation in current intensification between sites is possibly due to the limited polarisations and cavity resonances. This may explain why the intensification value for the wings (Figures 2.28(4) and 2.29(1)) shows overall an under test averaging -15 dB down, compared to the Cockpit (Figure 2.28(3)) which averages -5 dB.

The OATS results once adjusted in the same way have a span of around -8 dB to +8 dB as shown in Figure 2.31. The curves also show less variation versus frequency, as would be expected due to the absence of the numerous cavity resonances found in the TEM cell. However current variation between the observation sites limits the benefit of the scaling process here also.

Overall, if the TEM cell is compared to the OATS only in its TEM region and using the same polarisation, the accuracy is similar, although the OATS is marginally superior.

2.3.4 Eigencurrent Analysis

The CEM model of the Macchi aircraft contains 1739 triangles each with its own value of surface current density. In the above section this unmanageable number of current samples was reduced to seven, relating to areas of interest on the aircraft's skin. The choice however, of these observation sites, requires a number of assumptions to be made about the current distribution for them to be representative of the whole aircraft. Therefore if the surface current dynamics are non-intuitive, the results may not be representative of the overall surface current distribution of the aircraft. A method proposed by Leat [12], uses eigencurrent analysis to represent the surface currents as a series of fundamental current modes, where the most significant modes form a manageable sized set of data. This can be used to obtain a more complete picture of the surface current dynamics over the whole skin of the aircraft than is achieved using a few individual triangles.

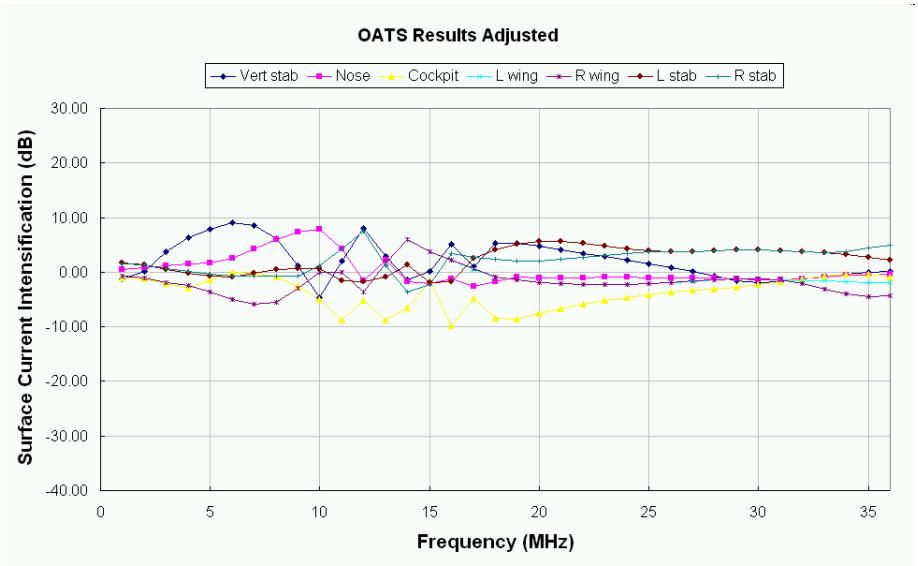

Figure 2.31: *Adjusted OATS+Macci surface current intensification curves for all 7 observation triangles.*

The current modes, proposed by Leat [12], can be divided into two categories: inductive (stimulated by the magnetic component of the incident wave); and capacitive (due to charge concentrations caused by the incident electric field). Within these two groups are a series of modes which are likely to appear on an aircraft type structure, these are listed in table 2.4.

The surface currents on the Macchi aircraft were calculated in Feko for the three scenarios, TEM cell, OATS and free space. Since the DSTO TEM cell is restricted to producing a vertical polarisation incident wave, the OATS and Free Space excitations were set to replicate this set-up. The Macchi aircraft was positioned in the TEM cell such that its tail lined up with the septum feed point and it's nose faced the septum load. The bow-tie antenna used as the radiator in the OATS case, was positioned aft of the aircraft to mimic the TEM cell orientation (see figure 2.32). In Free Space a vertically polarised plane wave source was used at an incident angle aft of the Macchi aircraft with a magnitude of 1 V/m. The TEM cell was calibrated by sampling the average empty cell electric field strength for a driving voltage of 1 Volt. The field was then scaled to match the 1 V/m incident field set in the Free Space case. The TEM cell model was therefore driven at 4.7 Volts as in Section 2.3.3. This calibration was performed at a frequency of 10 MHz in order to sample a region of pure TEM mode operation. To calibrate the OATS model the electric field strength was sampled at the Macchi's postion, but with the aircraft removed for the calibration. This produced a calibration curve of electric field strength versus frequency. The curve was used to adjust the Macchi surface current data for an incident electric field strength of 1 V/m. Note that in the OATS model, the MoM ground plane used in the previous sections was replaced by a perfectly conducting infinite standard Feko ground plane. This reduced the calculation time. Macchi aircraft surface currents were calculated in each case over the frequency range of 1 to 30 MHz at 0.5 MHz intervals.

The results for the Free Space calculation are shown in Figure 2.33. The results

Table 2.4: *The dominant capacitive and inductive modes which can be stimulated on the Macchi airframe.*

Eigencurrent Mode	Description	Type
531	Complex pattern of circulating currents, strongest is on the vertical stab and mid fuselage.	Inductive
532	Complex circulating fuselage current.	Inductive
533	Currents circulate in a horizontal plane around the fuselage.	Inductive
534	Counter rotating bands of current circulating about the fuselage axis.	Inductive
535	Mainly circulating current in the vertical stabiliser, however there is some horizontal plane fuselage current.	Inductive
536	Horizontal plane circulating currents on the forward half of the fuselage.	Inductive
537	Circulating current on the vertical stabiliser and around the fuselage axis at the leading edge of the wings.	Inductive
538	Complex current comprised of two helical fuselage streams flowing in opposite directions.	Inductive
539	Flows towards the nose on the upper fuselage and towards the tail on the lower fuselage.	Inductive
540	Similar to 539 but concentrated forward on the fuselage rather than aft.	Inductive
541	Circulating current around the pitch axis of the aircraft.	Inductive
544	Current which circulates on the fuselage in a horizontal plane.	Inductive
569	Circulating currents on the wings, rotating in the same direction on each wing.	Inductive
570	Circulating currents on the wings, rotating in opposite direction on each wing.	Inductive
571	Flows parallel to the fuselage axis, from tail to wings and nose.	Capacitive
572	Is the fundamental mode in the right wing. It flows parallel to the wing axis.	Capacitive
573	Is the fundamental mode in the left wing. It flows parallel to the wing axis.	Capacitive
574	Flows across the right tail-plane.	Capacitive
575	Flows across the left tailplane.	Capacitive
576	Vertical current on the vertical stabiliser.	Capacitive
577	Flows according to three charge concentrations, nose, tail and in-between the wings.	Capacitive
578	Flows according to four charge concentrations, nose, tail and two at intermediate fuselage positions.	Capacitive

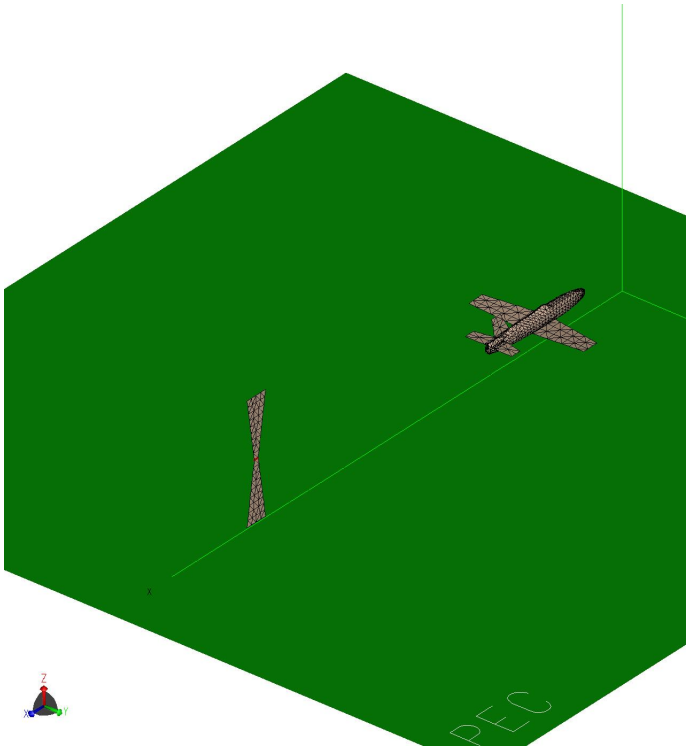

Figure 2.32: *Open Area Test site (OATS) configuration. A bowtie antenna is used to produce a vertically polarised incident field aft of the Macchi aircraft.*

represent the typical surface current distribution for an aircraft exposed to a vertically polarised wave while airborne. The eigenvector analysis shown in Figure 2.33 gives the relative amplitudes of the various eigencurrents excited as a function of frequency. In this case eigencurrent modes 539 and 541 are dominant from 1 to 10 MHz and from 17 to 23 MHz. This is not surprising since the horizontal magnetic field associated with the vertical electric field stimulates the circulating modes around the pitch axis of the aircraft. Overall the 539 and 541 modes vary only slightly in magnitude over the frequency range sampled. In the range between 10 MHz and 17 MHz the 571 capacitive mode dominates. This is due to the natural resonance of the aircraft fuselage plus wings. Above 23 MHz and below the 30 MHz sample maximum, the 576 mode steadily becomes dominant. This is the vertical stabiliser capacitive mode which is increasing in amplitude as the frequency approaches the natural resonance of the fin. The TEM cell and OATS techniques performance are measured against how closely they can reproduce this Free Space current profile.

The TEM cell model containing the Macchi, has an eigencurrent profile which is very peaky compared with the Free Space case. The eigencurrent analysis of the Feko results are shown in Figure 2.34 and Figure 2.35. Figure 2.35 is purely an enlargement of Figure 2.34. In comparing the TEM cell results with the Free space results (Figure 2.33), the dominance of the 539 and 541 modes are reproduced from 1 to 8 MHz and have the correct amplitude of 0.045. The 571 resonance mode is reproduced in the TEM cell case, peaking at the same frequencies as seen in the Free Space case. However, due to the high Q nature of the TEM cell cavity the resonance peaks are narrower than for Free space when considering the Full Width at Half Maximum (FWHM). This makes the two peaks

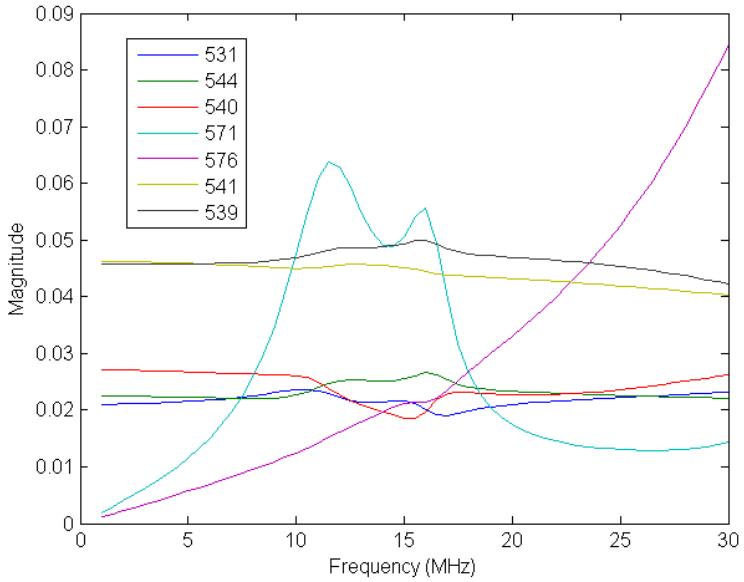

Figure 2.33: *Eigencurrent amplitudes as a function of frequency for the Macchi aircraft illuminated by an aft vertically polarised plane wave.*

at 12 MHz and 16 MHz respectively more distinct and over 20 dB higher in amplitude. The main discrepancy between the TEM cell and Free Space results is the excitation of the wing modes, 572 and 573, in the TEM cell case. This is due partly to the first order TE_{011} cavity resonance of the TEM cell coupling into the Macchi aircraft's wings as well as the higher Q of the wing resonance in a cavity. This interpretation could be tested with the application of active mode cancellation to the TEM cell system. Successful cancellation as described in Section 2.4, could potentially reduce the amplitude of these modes to more closely represent the Free Space eigencurrent profile shown in Figure 2.33. At frequencies between 23 to 30 MHz the 576 mode became prominent in the Free Space case, although present in the TEM cell it suffers from distortions from high order cavity resonances.

The eigencurrent analysis of the Macchi on the OATS is shown in Figure 2.36. Once again for frequencies between 1 to 8 MHz the 539 and 541 modes are reproduced as per the Free Space case. However, there is a 5 dB increase in the OATS case at the 2 to 3 MHz region. This is however only a minor effect which requires no further investigation. The 571 mode is the dominant feature of this OATS profile with an 18 dB increase in amplitude at 12 MHz compared with Free Space [3]. This is again due to the higher Q of the resonance due to the presence of a ground plane under the Macchi aircraft. The 16 MHz peak seen in the other two cases seems to be shifted up in frequency slightly to around 16.5 MHz. The 572 and 573 wing resonances are again present but 25 dB lower in amplitude than in the TEM cell case. This is due to the higher Q of a resonance in a cavity as compared with over a single ground plane. In essence, more of the energy is allowed to radiate for an

[3]The 18 dB over test for vertical polarisation is of the same magnitude as the 20 dB greater excitation of the 571 mode by horizontal polarisation [12]. This coincidence means that full field OATS sites which use only vertical polarisation, such as Pax River, may in fact be testing for horizontal polarisation levels, at least at the airframe resonance frequencies.

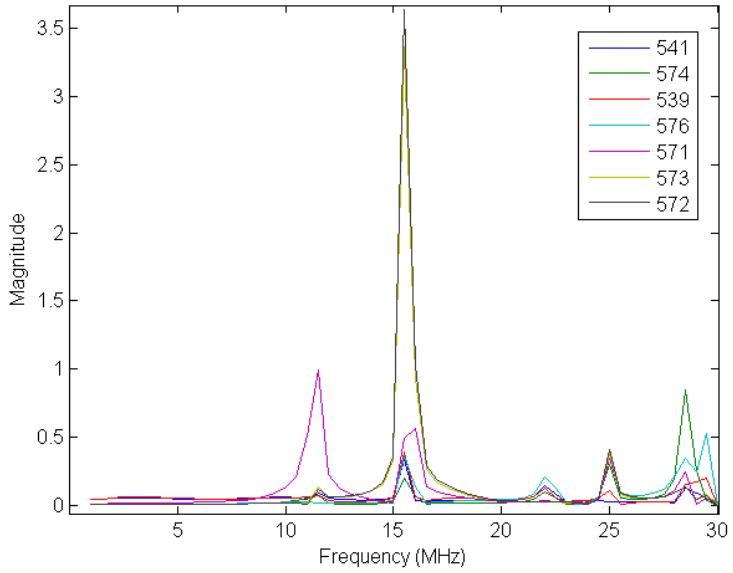

Figure 2.34: *Eigencurrent amplitudes as a function of frequency for the CEM calculations of the Macchi aircraft in the DSTO TEM cell.*

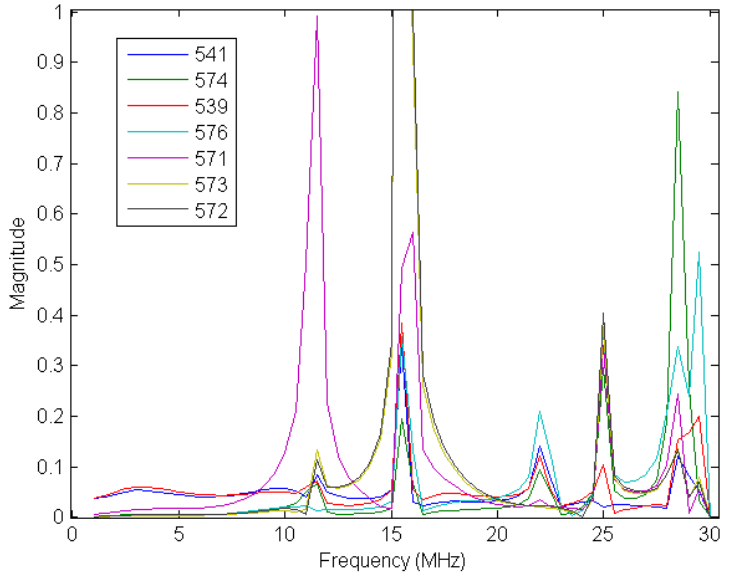

Figure 2.35: *Enlarged: Eigencurrent amplitudes as a function of frequency for the CEM calculations of the Macchi aircraft in the DSTO TEM cell.*

OATS. The 576 eigencurrent mode once more becomes prominent between 23 to 30 MHz. However, in the OATS case the amplitude peaks at 27 MHz and so is approximately 2 dB lower at 30 MHz than for the Macchi aircraft in Free Space.

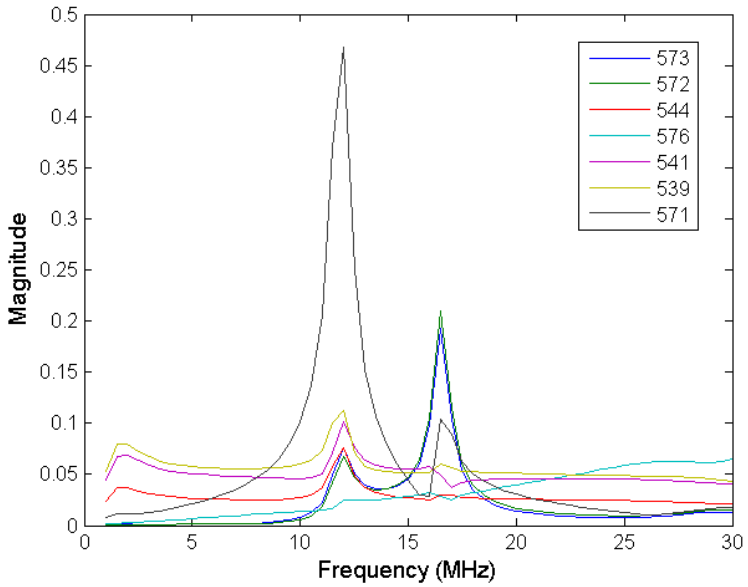

Figure 2.36: *Eigencurrent amplitudes as a function of frequency for the CEM calculations of the Macchi aircraft on the OATS illuminated by an aft vertically polarised wave.*

This discussion has identified the four modes which dominate the Free Space profile, the 539, 541, 571 and 576 modes. To give a clearer indication of how well the two testing techniques were able to reproduce these Free Space conditions, Figure 2.37 was generated. Note that 541 was not plotted due to its similarity to the 539 results and 572 was added since both TEM cell and OATS show strong resonance peaks for this and the similar 573. In the TEM cell and OATS cases the results for the modes just mentioned were divided by the relevant results for Free Space. On a logarithmic scale the 0 dB line represents a perfect reproduction of the current profile for the Macchi aircraft in Free Space.

The 539 eigencurrent mode which dominates below 8 MHz for the Free Space case is seen to be reproduced within 5 dB for both OATS and TEM cell. The TEM cell performs slightly better with less deviation from the 0 dB line below 8 MHz. Above 12 MHz the OATS method is seen to out perform the TEM cell with near perfect reproduction for most frequencies. The TEM cell suffers from the higher order resonances which were highlighted in Section 2.3.3.

Mode 571, which dominates the mid-frequencies is reproduced to a similar fidelity in both OATS and TEM cell up to 25 MHz. Again the TEM cell produces currents closer to the 0 dB line for frequencies below 10 MHz and the OATS for frequencies above 25 MHz.

The vertical stabiliser mode (576) which is excited at higher frequencies by the vertically polarised incident wave is reproduced equally by both methods below 10 MHz. Above this frequency the OATS is seen to easily out perform the TEM cell with near 0 dB results over the range. This distinction is replicated over the whole frequency range sampled for

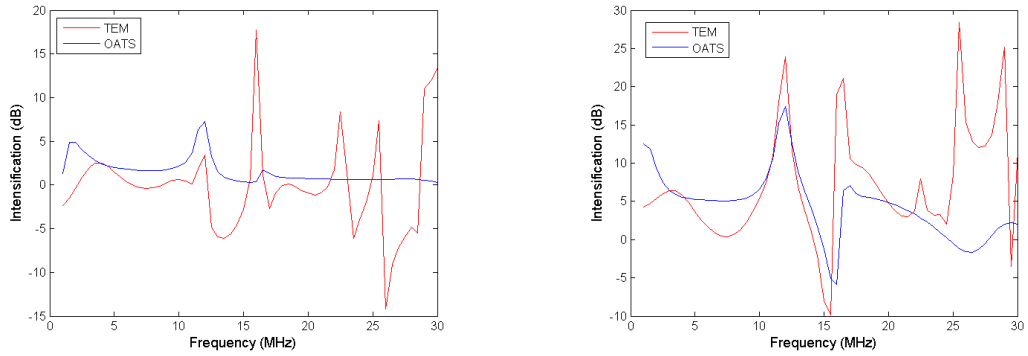

(1) 539

(2) 571

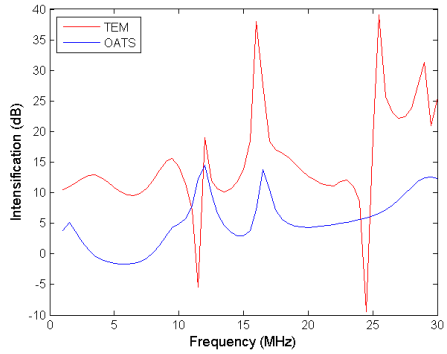

(3) 572

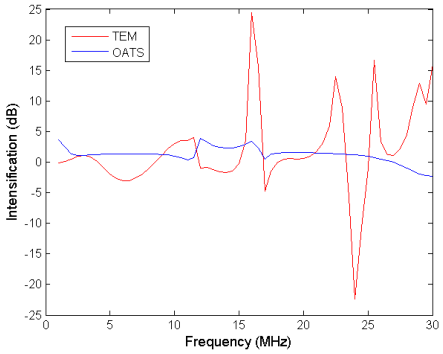

(4) 576

Figure 2.37: *Surface current intensification using an eigencurrent approach for the Macchi aircraft in a TEM cell and on the OATS. Results are plotted relative to the Free Space case. 0 dB indicates ideal.*

the wing mode 572. This mode is not excited in the Free Space case and so even a small excitation of the mode in the TEM cell is displayed as poor performance on the plot. These results confirm the conclusions made using the limited sample set of Section 2.3.3, whereby the OATS shows overall generation of surface currents on the Macchi aircraft closer to that seen for the Free Space case. This is particularly true for frequencies above 16 MHz where the TEM cell suffers from cavity resonances. However the TEM cell shows promise at frequencies below 16 MHz where in some cases it reproduced the Free Space current profile more closely than the OATS technique.

2.3.5 Conclusion

The performance of the TEM cell containing a Macchi aircraft has been assessed against a Macchi in Free Space and on an OATS. The performance was defined as the degree to which the technique could reproduce the electric field and surface current Free Space profiles. The comparison with the OATS was added to provide a performance comparison with a technique currently in use.

The electric field results indicated that the TEM cell method was able to reproduce

the Free Space conditions around the Macchi within accepted error margins for frequencies below 10 MHz. In some cases the TEM cell outperformed the OATS technique. For frequencies above 15 MHz the OATS technique clearly outperforms the TEM cell in reproducing the Free space field conditions. The TEM cell is limited in this frequency range due to amplification of the natural aircraft resonances and high order cavity modes.

The surface current investigations demonstrated similar trends as the field intensification results. It was evident however, that from comparing the two methods of current analysis that the eigencurrent method provides a higher fidelity of detail. This form of analysis is beneficial since it identifies the aspects of the aircraft structure which contribute the observed performance.

Overall it is clear that the TEM cell would benefit from a form of mode cancellation whether it be active or passive. This could potentially help it match the performance of the OATS at the higher frequencies. This together with the benefits of testing within an enclosure as opposed to testing outside, would make the TEM cell a technique which should be seriously considered. The over-testing at the airframe resonance relative to vertical polarisation should provide an effective test for horizontal polarisation at full field at the resonance peak.

2.4 Active Cancellation

2.4.1 Introduction

The non-TEM high-Q resonances, while desirable in reverberation chambers, create destructively high field levels making the chamber unsuitable for testing. The approaches used in the literature and in commercial TEM cells comprises various forms of passive absorber material, which may either be a ferrite or carbon loaded material [13]. To be well-coupled to the resonant modes, while not reducing the TEM mode, the absorber material needs to be appropriately distributed. It is often distributed over a terminating wall, as in the GTEM cell or behind carefully orientated wall slots [13]. While such methods are technically proven for equipment scale use, they are not the most economical for scaling up to the size required for a whole-aircraft test TEM cell. It is clear that the volume and hence cost of the material would increase with the cube of the TEM cell scale factor. Hill *et al* [14] attempted resonance suppression using longitudinal slots cut along the four corners of a TEM cell. However, limited success was found in eliminating all the targeted resonances. In addition, slots cut into the cell would re-radiate the energy outside the TEM cell, therefore causing RF spectrum issues. An alternative to passive solutions is active mode cancellation. When scaled up this method has the advantage of a much lower cost of implementation. This Section describes investigations into applying active mode cancellation to the DSTO TEM cell. In Section 2.3 the problem of high Q cavity resonances was highlighted as one of the restrictions on the TEM cell technique to reproduce the Free Space conditions for testing an aircraft. Active cancellation provides the opportunity, if successful, to reduce the distortion effect of these resonances and so extend the usability of the TEM cell.

2.4.2 Active Cancellation Using CEM Modelling

As an initial step into investigating the active cancellation technique the study focused on the TE_{011} resonance at 80 MHz (see Figure 2.16). The technique involved installing two half-loop antennas on the walls of the TEM cell. The half-loop antennas were J probes initially designed to measure the surface current on an aircraft's exterior. They are suitable for the active cancellation purpose since they can be orientated to inductively couple only to the TEM cell wall currents created by the resonance. The basic design is shown in Figure 2.38 with their location in the TEM cell shown in Figure 2.39. The half-loop antennas were used for the monitoring and injection roles in the negative feedback design. The idea was to measure the 80 MHz signal with one loop and then re-inject the signal with the other after a suitable phase change and gain has been applied.

The first step was to implement the concept into the CEM model of the TEM cell. Two half-loop antennas were constructed from Method of Moments (MoM) wire elements and added to the validated TEM cell model. A cut-away view of the MoM model is shown in figure 2.40. Both were added for completeness, however for the experiment only one was used. The electric field strength at 80 MHz was sampled once for the septum driven case and once for the injection loop driven case. The proportionality constants for both

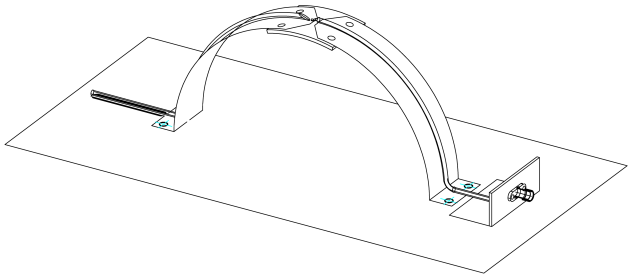

Figure 2.38: *Half-loop antenna.*

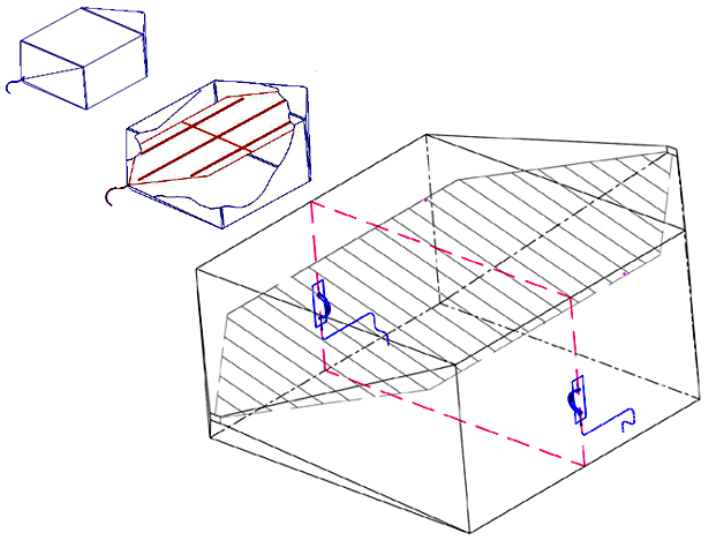

Figure 2.39: *The loop antennas were positioned on the walls on either side of the TEM cell, halfway between the floor and septum.*

cases can then be used to determine the applied voltage required on a half-loop antenna to cancel the resonance. The constants are written as:

$$k_{loop} = \frac{E_{loop}}{V_{loop}}; \tag{9}$$

and

$$k_{septum} = \frac{E_{septum}}{V_{septum}}. \tag{10}$$

Complete field cancellation at a centrally located test point could thus be achieved by using the value:

$$V_{loop} = \frac{-k_{septum}}{k_{loop}} V_{septum} \tag{11}$$

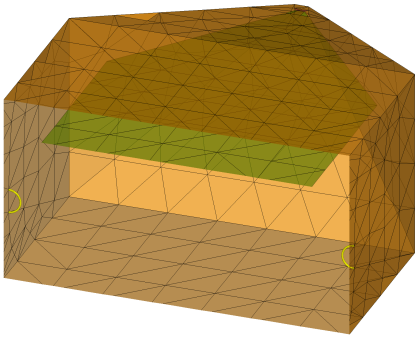

Figure 2.40: *The loop antennas were positioned on the walls on either side of the TEM cell CEM model, halfway between the floor and septum.*

for the loop drive voltage. k_{septum} however, contains contributions from the normal TEM mode as well as that from the resonance. Therefore the TEM mode constant, $k_{septum-TEM}$, must be extracted before the cancellation is applied otherwise it will be actively cancelled also. The electric field strength was calculated at frequency points either side of the resonance: at 71 MHz and 88 MHz, which are in regions of purely TEM operation (see Figure 2.41 red and green lines respectively). The average of the electric field strength for the two frequencies was used to approximate $k_{septum-TEM}$ similarly to equation (9). Thus, the resonance mode constant, $k_{septum-res} = k_{septum} - k_{septum-TEM}$. The voltage on the loop required for cancellation of the resonance field component alone is finally given by:

$$V_{loop} = \frac{-k_{septum-res}}{k_{loop}} V_{septum} \tag{12}$$

When this driving voltage was applied to one of the half-loop antennas, a 20 dB reduction was seen in the amplitude of the resonant field. The result, shown as the black line in Figure 2.41, resembles the pure TEM mode seen at frequencies calculated either side of the resonance. The results are also shown as a comparison between two electric field contour plots at 80 MHz, one with cancellation and one without (see Figure 2.42). The field plots show that with active cancellation the resonance field pattern in Figure 2.42(1) no longer dominates, leaving the TEM mode in Figure 2.42(2).

2.4.3 Modelling a feedback loop in the moment method

In the previous section, a drive voltage and phase was estimated based on the measured couplings to the resonant mode from the septum and cancelling loop separately. This corresponds to a feed-forward method. Like all feed forward methods it requires complete knowledge of these couplings over frequency. However in this case, this may not be practical as the couplings will change with the installation of the EUT into the TEM cell.

A more practical approach is to use a feedback method. Such an approach attempts to bring the error signal (in this case the resonance amplitude) to zero automatically, provided

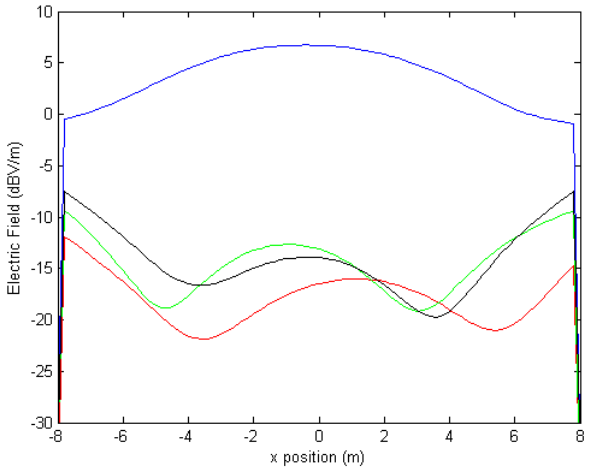

Figure 2.41: *Electric Field transverse to propagation direction in the TEM cell at the midpoint between septum and cell floor for various frequencies. The Blue line at f=80 MHz shows the cosine-like variation of the uncancelled TE_{011} mode which swamps the TEM mode. The Black line also at f=80 MHz shows the effect of active cancellation. The red line at f=71 MHz and the Green line at f=88 MHz show adjacent pure TEM mode fields.*

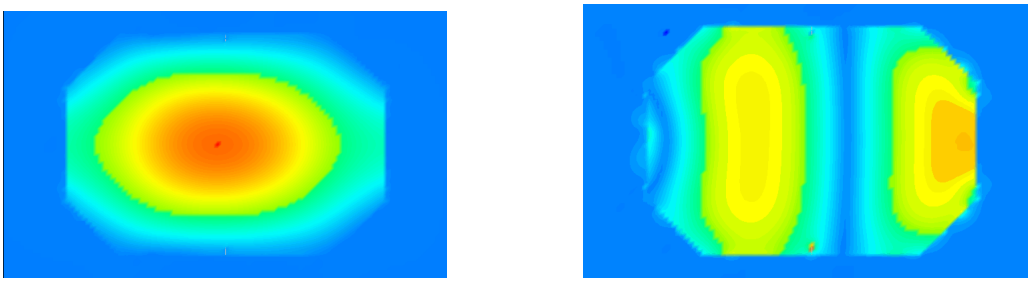

(1) Without Cancellation (2) With Cancellation

Figure 2.42: *Horizontal Electric Field slices through the TEM cell between septum and floor at f=80MHz. The plots have arbitrary scales, different in each case. Red indicates highest field magnitude.*

stability criteria are met. The stability criteria are fully described in the experimental Section (2.4.4). In this section, some work is described that demonstrated the feasibility of the feedback approach in the moment method model. A full stability analysis was not undertaken, but rather, a single gain and phase value was intuitively derived, and proved modestly successful.

The feedback concept, as applied here, is based on an amplifier and phase shifter chain with input taken from one loop and output fed to the other. The input loop serves to monitor the resonance level, and hence the error level. If the input loop is fed to a 50 Ω cable the input voltage to the amplifier/phase shifter chain is given by:

$$V_n = 50 I_n \tag{13}$$

Where I_n is the current on the input loop (measured at segment n). The feedback loop would apply a voltage to the second loop (at segment m):

$$V_m = G e^{i\phi} 50 I_n \tag{14}$$

Now, the ratio V_m/I_n for a successful feedforward mode cancellation at a single frequency point may be taken from the previous section example, by taking the loop applied voltage and the computed input loop current from the solution, and was found to be:

$$V_m/I_n = 50 G e^{i\phi} \sim 1E3 e^{i0.87} \tag{15}$$

Comparing this to the earlier equation, we see this corresponds to a gain, G, of 20, or 26 dB.

The next consideration is how to apply the idea of feedback within a moment method model. How can the amplifier and coaxial cables etc, be represented? Moment method models typically are designed to represent passive devices.

One elegant way of doing this is by a simple modification of the relevant element of the moment matrix. Readers familiar with the Harrington approach will be aware that the matrix element $Z_{m,n}$ is the voltage induced on the *mth* element by a unit current on the *nth* element considered to be acting alone. The $Z_{m,n}$ element represents the propagation through free space of the EM wave from the short dipole *nth* element to the short receiving dipole *mth* element when computed by the conventional moment method. We can add a second propagation path between these two elements alone, through active elements and coaxial cable by simply adding the V_m/I_n calculated above to the passively calculated matrix element:

$$Z_{m,n}^{feedback} = Z_{m,n}^{Harrington} + 50 G e^{i\phi} \tag{16}$$

In practice, as the added feedback component is many orders of magnitude larger than the original element, it is sufficient to replace it with the feedback component.

This method was applied by exporting the FEKO matrix at each frequency, modifying the relevant element (m=783, n=863), and then computing the current vector. The results of this can be seen in figure 2.43. It is seen that the feedback has reduced the resonance peak field from 6 dBV/m to -8 dBV/m. The performance is not perfect, as the null is not removed, although reduced in depth. This may be attributed to the choice of feedback phase. This work confirmed the feasibility of the feedback approach to the control of the injected signals amplitude and phase. A complete stability analysis would require consideration of Nyquist's criteria, and was applied to the scale model experiments in the following sections.

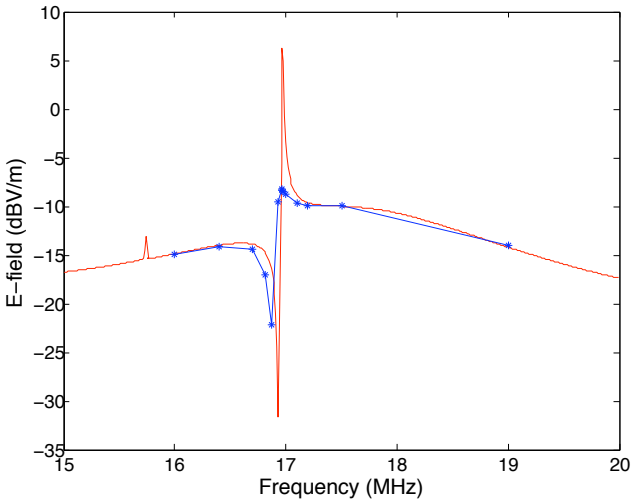

Figure 2.43: *FEKO modelling of active cancellation in the DSTO TEM cell. Focused on the TE_{011} resonance. Red line: Feko model without cancellation, Blue line: with cancellation.*

2.4.4 Designing a Feedback System

In applying the active mode cancellation in practice the TEM cell becomes part of a negative feedback system. The two half-loop antennas shown in Figure 2.39 are used by assigning one to measure surface currents and the other to inject the cancellation signal. The two antennas were connected on the outside of the TEM cell via a feedback loop which performed the necessary amplification and phase changing.

In designing this negative feedback system a major consideration during the design process was stability. The values of gain and phase utilised as part of the feedback loop can set the system into oscillation if chosen incorrectly. The well known Nyquist stability criterion was used in this case to determine which combinations of phase and gain could be used to ensure stable negative feedback. To aid in this design process the TEM cell feedback system was represented as a schematic diagram (Figure 2.44) of the type normally used in control theory analysis. The definition of the blocks and labels in the schematic are listed in Table 2.5. The cancellation part of Figure 2.44 can be represented in a simpler form by defining two transfer functions describing the coupling through the TEM cell. Consider the physical system where we are able to measure the signal in the error loop due to the septum in addition to the signal in the error loop due to the injection loop. We define these quantities as M and G respectively of the form:

$$M = \gamma_{TE_{011}}\alpha\beta = \left.\frac{V_{error}}{V_{sept}}\right|_{V_{inj}=0} \tag{17}$$

$$G = \beta^2\alpha^2 = -\left.\frac{V_{error}}{V_{inj}}\right|_{V_{sept}=0} \tag{18}$$

The voltage V_{error}, can therefore be represented as a function of the V_{sept} and V_{inj} by defining the transfer function given by:

$$V_{error} = M.V_{sept} - G.V_{inj} \tag{19}$$

Since $V_{inj} = A.e^{i\phi}V_{error}$ then equation (19) becomes:

$$V_{error} = \frac{M}{1 + GA.e^{i\phi}}V_{sept} \tag{20}$$

Note that at the most stable combination of $G.A$, i.e. when their combined phase is 0°, equation (20) becomes $V_{error} \approx M/|GA|V_{sept}$. Since without the feedback loop, $V_{error} = MV_{sept}$ by definition of M, we see that the suppression of the resonance mode is $\approx 1/|GA|$. This form can be used to quickly estimate the degree of attenuation of the resonance amplitude for a certain feedback loop gain.

The Nyquist criterion for the TEM cell feedback system requires that for stability $|GA| < 1$ when its phase is 180°. The complex quantity G was measured using a Vector Network Analyser (VNA) connected between the two half-loops over the range 80-83 MHz at 2.5 kHz steps (see Figure 2.45). Then $|GA|$ was calculated using values of A from 0 - 60 dB and ϕ from 0 - 360°. The results are shown in Figure 2.46. A Nyquist plot for a single unstable case for $A = 50$ dB and $\phi = 55°$ is shown in Figure 2.47

Using Figure 2.46 as a reference, an external feedback loop with a gain of 40 dB which provides a phase change of 270° will produce a stable negative feedback system with approximately 23 dB of attenuation to the resonance amplitude. Knowing the gain required, we can determine the series of amplifiers required for the feedback loop. However the power requirements also have to be a consideration to locate the active equipment within its operational range. The power requirements can be found by comparing the two quantities M and G. The results are plotted in Figure 2.45.

The results in Figure 2.45 show that at the measured resonant frequency, 81.3 MHz, the ratio M / G = -11 dB (Note the 2 MHz variation between the resonant frequency between model and measurement seen also in Figure 2.16). This means that for 100 W applied to the septum the required power on the injection half-loop to cancel the resonance is 7.2 W. The next step was to use this value with the phase and gain figures from Figure 2.46 to design the necessary combination of low noise and power amplifiers, attenuators and cable lengths in the feedback loop.

2.4.5 Physical Design

The design of the feedback system was based on the 7.2 W injection power quoted above, assuming a septum input power of 100 W. The feedback loop was designed to provide an overall gain of approximately 40 dB and a phase change close to 270°. Attenuators were used in conjunction with the power amplifiers to protect the amplifier inputs should the cancelling not be successful, and the input power to the feedback loop be higher than expected. Cable lengths were varied in order to tune the phase of the chain. The initial

Table 2.5: *The definitions of the components in the control schematic diagram in figure 2.44. All values are complex functions of frequency. Electric field values are located at a single point in space.*

Name	Definition
E_z^{TEM}	The z component of the Electric field due to the normal TEM mode.
E_z^{Total}	The total electric field in the z direction after mode cancellation.
$E_z^{TE_{011}}$	The electric field in the z direction due to the TE_{011} resonant mode.
$E_z^{TE_{011}-error}$	The residual electric field in the z direction due to the cancellation of the TE_{011} resonant mode.
$E_z^{TE_{011}-inj}$	The electric field in the z direction injected to cancel the TE_{011} resonant mode.
J_z^{error}	The surface current density measured in the error loop which is due to $E_z^{TE_{011}-error}$
J_z^{inj}	The surface current density injected by the error loop which produces $E_z^{TE_{011}-inj}$
V_{error}	Voltage measured on the error loop which is due to J_z^{error}
V_{in}	Input signal to power amplifier
V_{inj}	Voltage on injection loop
V_{sept}	Septum driving voltage
α	The transfer function between $E_z^{TE_{011}-error}$ and J_z^{error} and the reciprocal path J_z^{inj} and $E_z^{TE_{011}-inj}$.
β	The reciprocal transfer function between J_z and V for a half-loop antenna.
γ_{mode}	The transfer function which produces a particular electric field strength of the type 'mode' from a given V_{sept}.
A	The gain of the external feedback loop
ϕ	The phase of the external feedback loop

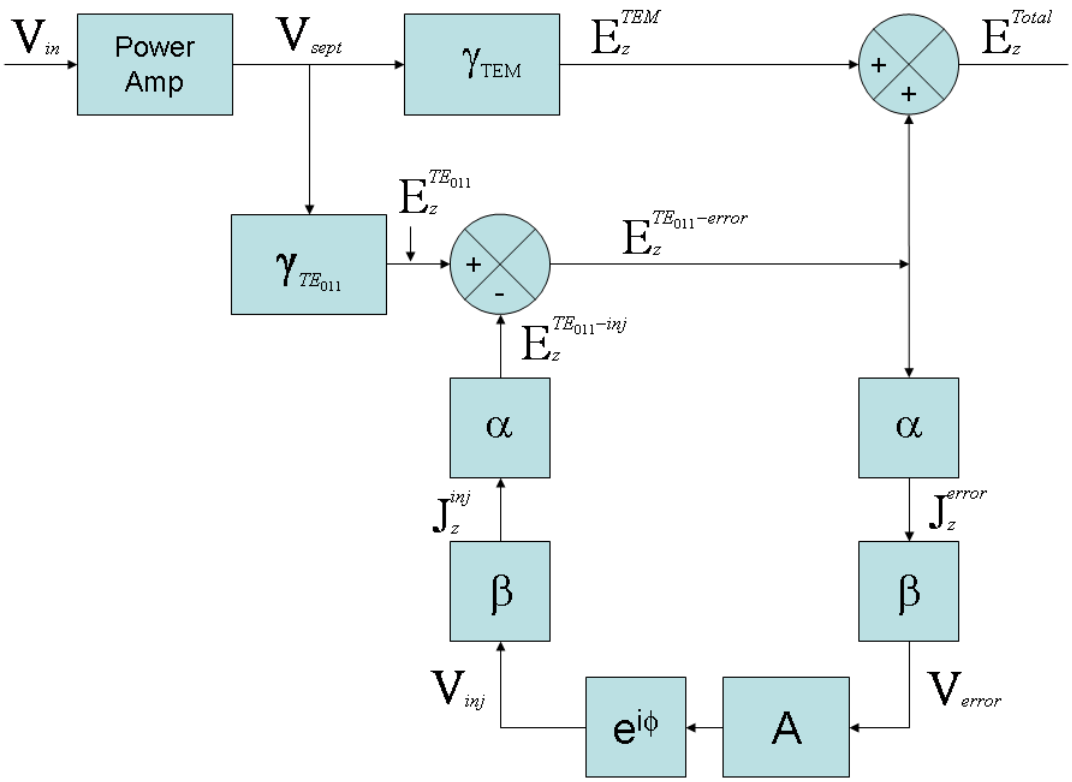

Figure 2.44: *Schematic representation of the negative feedback control system designed for active cancellation of the TE_{011} resonant mode in the TEM cell.*

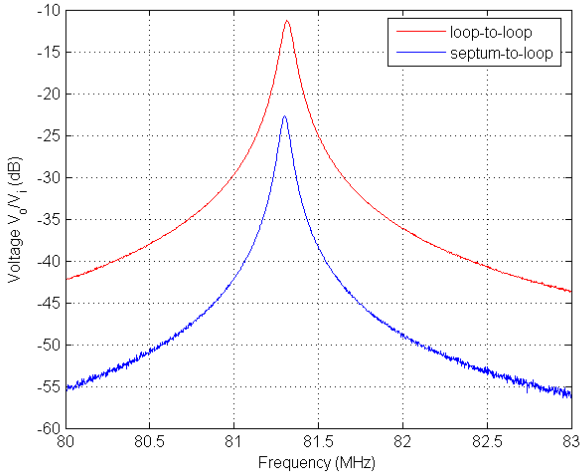

Figure 2.45: *Shows the loop-loop coupling G, and the septum-loop coupling M. At the resonant frequency of 81.3 MHz the ratio between M and G is -11 dB.*

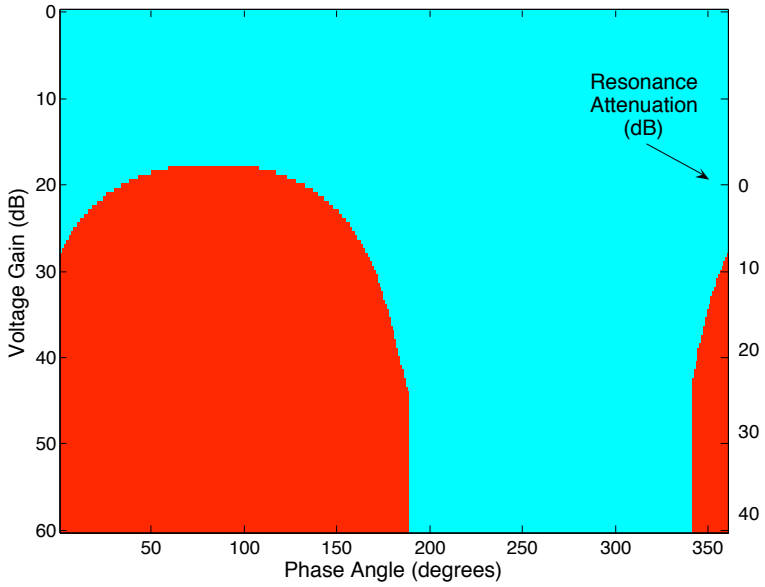

Figure 2.46: *Feedback loop stability plot calculated for A = 0 - 60 dB and ϕ = 0 - 360°. The regions marked in red indicate areas of instability.*

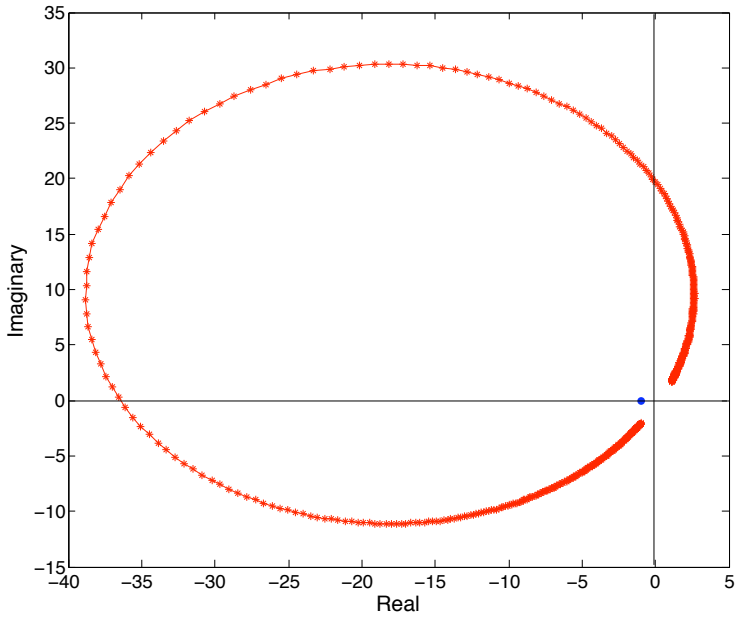

Figure 2.47: *Nyquist plot calculated for A = 50 dB and ϕ = 55°. This is an unstable combination of G and A since $|GA| > 1$ at 180°*

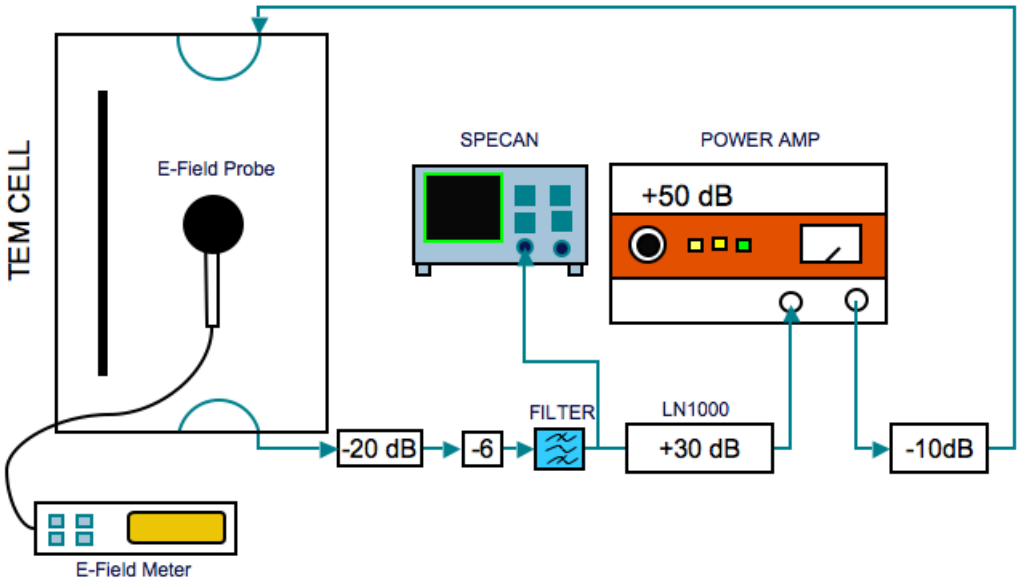

Figure 2.48: *Feedback system design schematic.*

design is shown in Figure 2.48. The filter depicted in Figure 2.48 as part of the feedback chain was initially an 80 MHz band-pass filter with a 5 MHz bandwidth.

A VNA was used to measure the gain and phase characteristics of the feedback chain for 1200 evenly spaced frequency samples between 80 MHz to 83 MHz. Using the cables available, a phase of 255° was achieved at 81.35 MHz. This value varied with frequency either side of the resonance. The transfer function was measured between the two half-loop antennas installed in the TEM cell over the same frequency range. The gain and phase characteristics of the feedback chain were analysed using the Nyquist Stability criterion to assess the stability of the physical system. The Real and Imaginary parts of the GA product are plotted in Figure 2.49. Each pair of Real and Imaginary points corresponds to the GA product calculated at a particular frequency.

The Nyquist stability criterion requires that for stability $\Re(GA) < 1$ when $\Im(GA) = 0$. With this in mind, Figure 2.49 shows that the point (1,0) is just encapsulated within the stability curve. This translates to the system being marginally unstable. A phase gradient of 100° from 80 MHz to 83 MHz, which was introduced by the band-pass filter was thought to be the cause. The filter was therefore removed to reduce the phase gradient. However, high order TEM cell cavity resonances (at 915 MHz) consequently appeared, which were not controlled by the 81.35 MHz cancellation system. It was clear that a filter was required to limit the effect from high order resonances. Initial experiments were carried out with the band-pass filter, keeping a close watch on the systems stability.

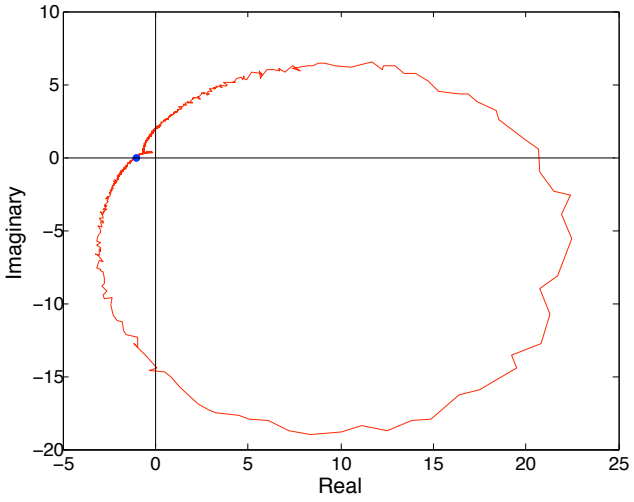

Figure 2.49: *Nyquist stability plot for the feedback chain containing the band-pass filter (red line). The blue star represents the (-1,0) point.*

2.4.6 Results

Again, all experiments were carried out from 80 MHz to 83 MHz, and utilised the 80 MHz bandpass filter with the 5 MHz bandwidth. Initially a spot frequency test was used to gauge the effectiveness of the active cancellation system on the TE_{011} resonance in the empty TEM cell. Electric field strength measurements were made using a field probe placed at a central point within the TEM cell's test volume at 80 MHz, 83 MHz and 81.35 MHz. The 81.35 MHz point corresponded to the TE_{011} mode. For safety, a reduced septum input power of 25 W was used for this test instead of the 100 W used in the design stages. In each case the power on the septum is engaged initially. Then the power amplifier gain is increased gradually while monitoring the signal in the feedback chain using a spectrum analyser (see Figure 2.48). In this way instability in the feedback system can be identified early and the power amplifier disengaged. Table 2.6 lists the results.

Table 2.6: *This shows the electric field results from the active cancellation spot frequency checks. With an without the active cancellation system active.*

Frequency (MHz)	E Field (V/m) - no cancellation	E Field (V/m) - with cancellation
80	21.5	no change
81.35	130	26.5
83	29.2	no change

The results in table 2.6, show a 13.7 dB attenuation in the electric field strength at the 81.35 MHz frequency point. For 25 W on the septum this required 1.8 W applied to the injection loop. However, there was no need to control this as it was all done by the feedback loop.

The spot frequency experiment demonstrated the expected level of resonance attenuation. The logical progression was to test the system over a range of frequencies thereby monitoring the stability. Equipment was again set-up as per Figure 2.48. The septum was powered over the frequency range of 80 MHz to 83 MHz divided up into 52 samples. The frequency samples were distributed in order to provide higher fidelity over the resonance peak bandwidth compared with the TEM mode regions. At each frequency point the septum input power was given a low initial value of around 10 W. The power was then incrementally increased while monitoring the TEM cell central electric field levels. This ensured that the fields inside the TEM cell would not exceed the 300 V/m limit of the field probes and so avoiding any damage to the probes. Septum input power was typically 100 W over the frequency range except at the resonance frequencies where the power was kept slightly lower. Final results were obtained by normalising the electric field levels using the total input power for each frequency. The net input power P_{net}^{sep} is given by:

$$P_{net}^{sep} = P_{fwd}^{sep} - P_{rev}^{sep} \tag{21}$$

where P_{fwd}^{sep} is the forward power measured at the septum input and P_{rev}^{sep} is the measured reverse power. The electric field strength is normalised by P_{net}^{sep} to give $\mathrm{V/m/W^{\frac{1}{2}}}$. The results are given in Figure 2.50, where the case with no cancellation is given in red, while the case with cancellation is given in green. The results show a $\sim$ 17 dB attenuation of the resonance field at 81.35 MHz. However, from 81.6 MHz to 82 MHz a broad peak is seem. This seems to be the result of instabilities caused by the negative feedback system moving into a region of regenerative oscillation due to the marginal stability here. This was represented by the marginal stability shown in the Nyquist stability plot for the feedback chain, Figure 2.49. This hypothesis was tested by reducing the power on the feedback amplifier and then re-running the experiment. The results are shown as the blue curve in Figure 2.50. As a result, the instability peak is removed. However, the $\mathrm{TE_{011}}$ is only attenuated by 8 dB instead of 17 dB.

In order to obtain an electric field profile, which represents near constant TEM operation over the 80 MHz to 83 MHz range, an adaptive approach needs to be implemented. This could be in the form of a programable attenuator, which would be used to limit the cancellation systems output to TEM cell resonance region only. This process was investigated by repeating the above frequency sweep experiment with varying degrees of attenuation in the feedback system. A plot of the results is shown in Figure 2.51.

The varying attenuation results (Figure 2.51) suggest that a near constant TEM mode of operation can be achieved by transitioning from one curve to another over the frequency range. Specifically this could be achieved by following the "0 dB" curve (green line) below 81.65 MHz and then following the "Cancel Off" (black line) above 81.65 MHz. In essence this suggests disengaging the active cancellation system above 81.65 MHz or applying an appropriate level of attenuation. The result would be a near constant TEM field of 6 V/m from 80 MHz to 83 MHz with a gradual increase peaking at 4 dB above the TEM level at 81.65 MHz. This is a manageable increase in field level in a testing environment, and could be negated further with a slight adjustment to the septum input power at the appropriate frequencies.

How does the active cancellation system perform with a loaded TEM cell rather than

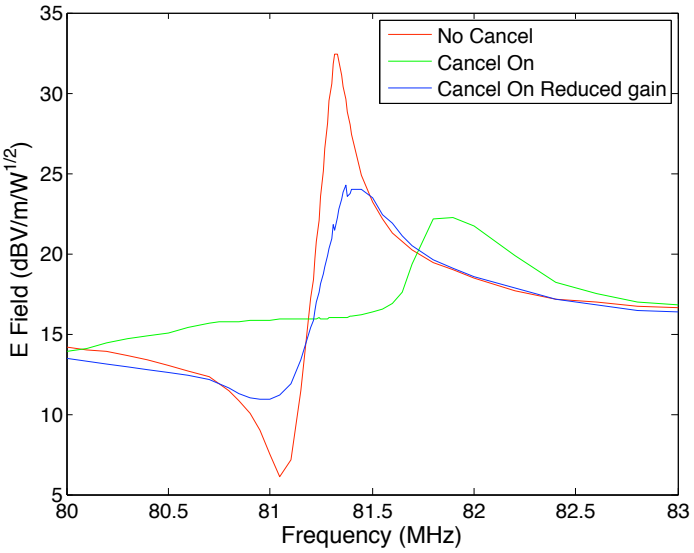

Figure 2.50: *Effect of active cancellation on the TE_{011} resonance as a function of frequency.*

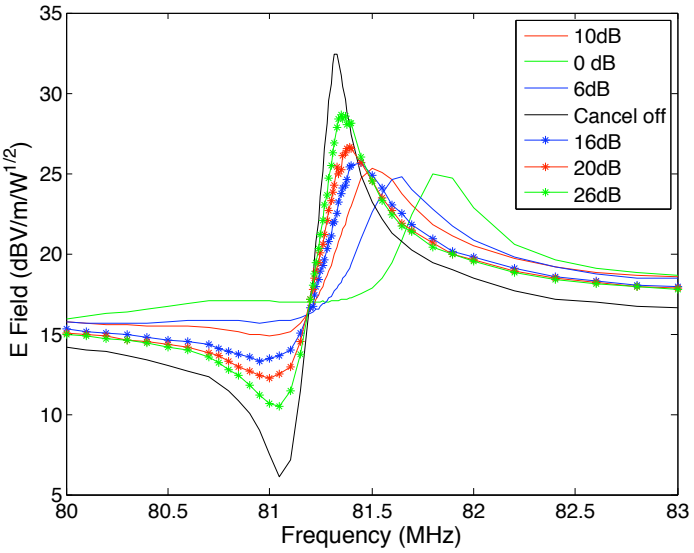

Figure 2.51: *Effect of active cancellation on the TE_{011} resonance as a function of frequency with varying degrees of attenuation in the feedback system. The results with the active cancellation system active for varying degrees of attenuation are identified in the legend by the level of attenuation.*

the empty cell? A aircraft shaped aluminium object, "planeoid", was used to load the DSTO scale TEM cell for testing the active cancellation system. It was placed in the TEM cell in an orientation based upon the intended testing setup. With the active cancellation system active, the electric field sampled by the field probe was recorded as a function of frequency from 80 MHz to 83 MHz. The results are shown in Figure 2.52.

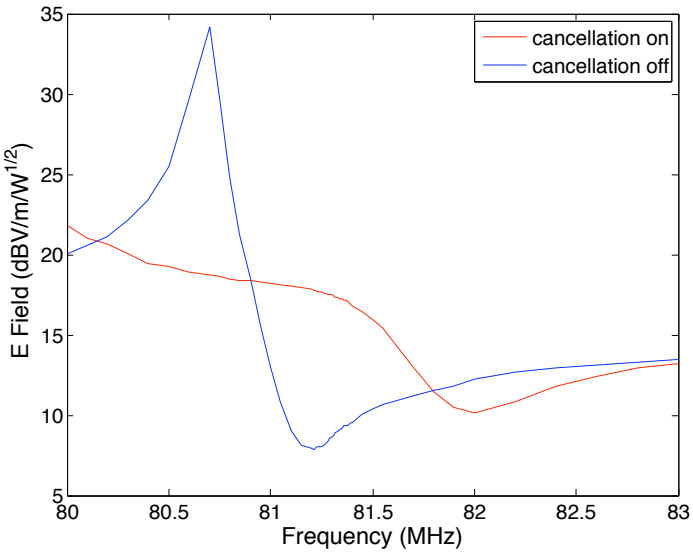

Figure 2.52: *Active cancellation applied for a loaded TEM cell. Shows comparison electric fields for when the cancellation system is active and inactive.*

For the case where the planeoid was added to the TEM cell, with the cancellation inactive, the 81.35 MHz TE_{011} resonance was shifted down in frequency to 80.7 MHz. Once the cancellation system was activated the resonance peak was reduced by 14 dB down to the TEM mode of operation. However, the slow increase in the electric field strength as the frequency approaches 80 MHz, suggests a possible move to regenerative oscillation outside of the frequency range sampled. This result suggests that the active cancellation loop phase requirements are relatively insensitive to loading conditions.

2.4.7 Conclusion

With the aid of CEM modelling and the Nyquist stability criterion, a system was designed to attenuate the TE_{011} (81.35 MHz) resonance within the DSTO TEM cell. Modelling indicated a possible 20 dB attenuation in the resonance field, using the half loop antennas orientated to couple to the induced surface currents. Investigations into the proposed design suggested a marginally stable system due to the phase gradient imposed by the bandpass filter. This was however, unavoidable since the filter was required to suppress the field contributions from higher order cavity resonances and low frequency septum resonances. The active cancellation system was subsequently tested over the frequency range 80 MHz to 83 MHz. Results showed a 17 dB reduction in the amplitude of the resonance field. However, an instability in the feedback system was seen as a peak in

the field at around 81.7 MHz. Further investigation suggested that the solution to the instability is to remove the active cancellation system for frequencies other than the TE_{011} frequency. This could be achieved by using a programmable attenuator which would apply the appropriate degree of attenuation at the correct frequency. Results showed that this method has the potential to provide a near constant level of TEM operation over the frequency range investigated. This same level of performance also seems attainable when the TEM cell is loaded with a test object.

Chapter 3

An RC/TEM Hybrid Facility

3.1 Introduction

In Chapter 2 the TEM cell concept was shown to have the potential to provide a test environment for whole aircraft EMV investigations. The next step is therefore to optimise the TEM cell design for integration into the DSTO reverberation chamber (RC) to form a 10 kHz to 18 GHz hybrid EMV test facility. Other groups which have studied the possibility of a hybrid RC/TEM facility found that the major drawback was the existence of a transition region [8, 9, 10] between TEM and RC operation. In this region field characteristics were found to be too erratic to be suitable for providing a EMV testing environment. However, in Section 2.4 it was shown that we have made progress to allow testing in the transition region. So how practical a proposition is it to build a RC/TEM hybrid facility?

Firstly, the requirements of such a testing facility must be assessed. The overall aim is to add a 10 kHz to 30 MHz EMV testing capability to the current DSTO RC. Below are the requirements:

- Produces near MIL-STD-464A test levels. This would remove the need for low-level-swept measurements and bulk-current-injection.
- Provides near continuous access to the RF spectrum below 30 MHz.
- Minimal degradation of the RC operation.
- Easy to move aircraft in and out of facility.
- Protection for aircraft in the event of an equipment malfunction.
- Quickly assembled when required, limiting the aircraft's out-of-service time and minimising costs (eg. salaries for subject experts)

The complete design is the subject of future research, however we will describe the major cost drivers including power amplifier requirements and possible physical design solutions.

3.2 Design

3.2.1 Physical Design Solutions

The current size of the DSTO RC is 29 x 11 x 6 m. This has been extended from its original length of 21 m, which was the size used when considering the dimensions of the scale DSTO TEM cell. If the dimensions of the 1:4.7 scale TEM cell are scaled to their intended size, we find that the cell easily fits inside the current DSTO RC. This is shown schematically in Figure 3.1. The Macchi aircraft is added to Figure 3.1 in order to gauge the size of the facility.

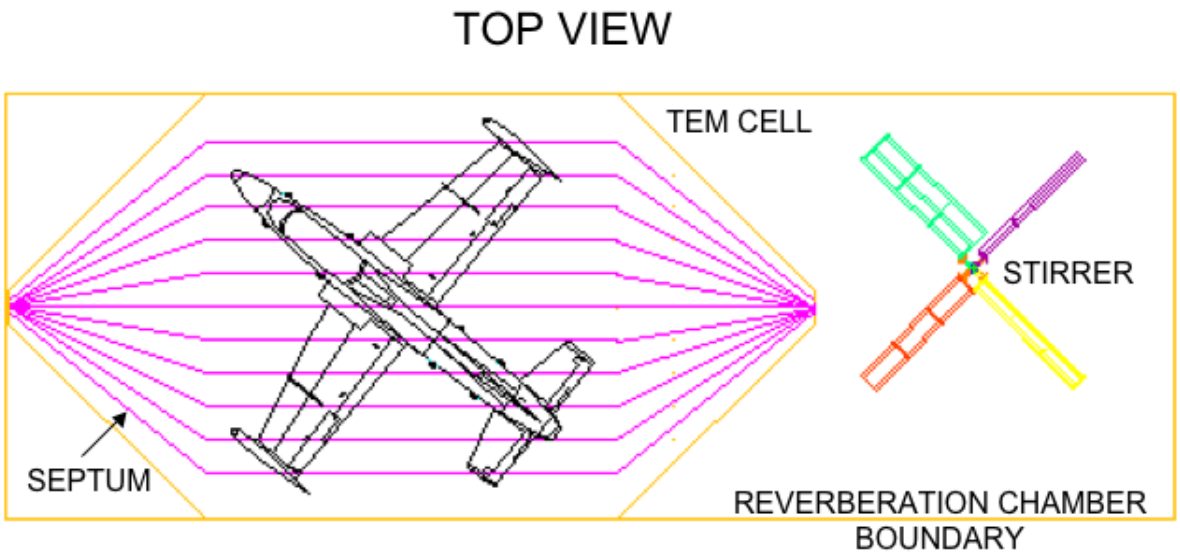

Figure 3.1: *A schematic of the proposed RC/TEM Hybrid facility*

3.2.1.1 Septum

To reiterate, the scale TEM cell utilised a solid aluminium septum 4.48 m long and 1.83 m at its widest point. When scaled up to its intended size, 4.7 times larger, these dimensions become 21 m and 8.6 m respectively, with a surface area of $\sim$135 m^2. Considering the required skin depths for aluminium and steel (Fe) over the frequency range of interest (Figure 3.2), 0.5 mm sheeting fixed to a tubular frame work could be used to construct a full sized solid septum. This sheet alone has a mass of nearly 175 kg for aluminium and 500 kg for steel. This is however without the weight of the supporting framework which could be of the order of 1.5 tonnes. If installed in the DSTO RC, the septum would

lay horizontally 1.4 m from the ceiling and would be suspended using non-conducting supports.

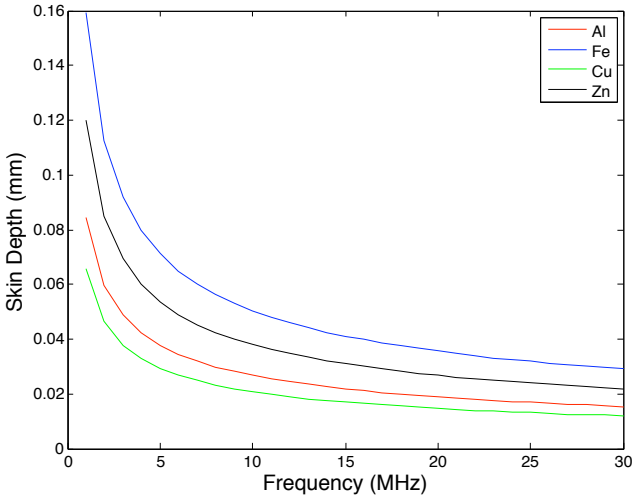

Figure 3.2: *Skin depth as a function of frequency for various metals. Where* μ_r*=1 and the resistivities used were* ρ_{Al}*=2.82E-8* Ωm*,* ρ_{Fe}*=1E-8* Ωm*,* ρ_{Cu}*=1.7E-8* Ωm*,* ρ_{Zn}*=5.68E-8* Ωm*.*

An alternative is to use a septum constructed from cables. Wire septums are reported in the literature [15], and provide increased field uniformity compared with solid. All the cables would be driven with the same signal (magnitude and phase), and their spacing chosen to be smaller than the separation between the septum and the aircraft-under-test in order to limit field distortions. As an estimate, eleven cables could be used each fitted with 550 Ω making a combined load of 50 Ω. The load is distributed amongst the cables in an attempt to attenuate any septum resonances which could potentially be generated around the loops within the structure.

For both septum designs a requirement is to not disrupt the reverberation mode of operation. This would be achieved by isolating the source and load from the septum. Also the proposed TEM cell design only generates vertically polarised waves. More investigation into the generation of horizontally polarised waves is required. Other groups have used multiple septa to obtain multiple polarisations and aspect angles [16], however in an aircraft sized facility these design options prove difficult. Similar limitations in the generation of horizontally polarised waves is found on an OATS, where efficiencies are low due to the presence of a horizontal ground plane. In fact many test houses test use only vertical polarisation [4].

3.2.1.2 Tapers

The classical TEM cell design [4] calls for tapered regions at either end of the cell converging on the feed and load points of the septum respectively. These tapers graduate

[4]For example at Pateuxent River, the US Navy uses a vertically polarised antenna for its full field testing at HF

the impedance transition from coaxial transmission line to TEM cell. Departures from the classical TEM cell design have however been shown to provide the required field environment for testing. The WTEM reported in [15] employs a single taper design with termination achieved on a non-tapered wall using a resistor array into RF absorber material. Others have removed the tapers completely as in the 3-D TEM cell reported in [16]. The desire is to achieve TEM operation which provides the required reproduction of free space conditions, but allowing some flexibility in the physical design.

If required however, the tapered sections could be constructed from lightweight building products formed into four triangular sections either end of the cell. The sections could be hinged to the RC walls in order to provide non-intrusive storage during RC operation and rapid erection when required. It is not necessary for the triangular sections to be of continuous sheet construction. Generally, provided the maximum circumference of any aperture on a conducting mesh is less than $\lambda/10$, the mesh appears as a continuous sheet to RF. A possible solution involving catenary cables and lightweight mesh could also be considered, as geometric exactness is not essential to the operation of the TEM cell. In all the options available the practical factors to consider include rolling an aircraft over any lower panels, ease of construction, minimal modification required to the basic RC structure and low impact upon RC operation.

3.2.2 Electronic Design Solutions

3.2.2.1 Powering the Septum

The TEM cell component of the RC/TEM facility is intended to operate in the 10 kHz to 30 MHz frequency range. In MIL-STD-464A the maximum external EME for most situations in this band is 200 V/m (rms) peak and average. For the proposed hybrid facility a power of 28 kW is required on the input of the septum to achieve this field level. Powers of this magnitude are difficult to deal with and amplifiers difficult to source. A compromise is to run the test at a lower field level. A 10 kW amplifier is readily available which operates in the 100 kHz – 250 MHz frequency range. This would produce a nominal field level of above 100 V/m. Although this is 6 dB below the MIL-STD field levels, it is 40 dB higher than is available on the DSTO OATS. The TEM cell therefore could provide a degree of full field EMV testing above that already achieved at DSTO in the 10 kHz to 30 MHz frequency range.

Also required for septum operation is a form of high power RF termination. In the case of the solid septum only a single 50 Ω load is required. The load must be power rated to 10 kW. With this comes special considerations when designing the connection point to the septum. A load rated to 10 kW can be quite large in size, eg. 560 × 400 × 400 mm with a weight of 50 kg. The load could be installed above the RC ceiling in the roof space. The load would also require 240 V power to operate its cooling systems. If the multi-wire septum option is chosen a high power load must be purchased for each cable. In the 11 cable example mentioned above, each 550 Ω load would require a power rating of approximately 1 kW. In both solid and multi-wire easy access to the loads must be made such that they can either be removed or isolated during RC operation.

3.2.2.2 Dealing With Resonances

The DSTO RC provides an acceptable test environment down to a frequency of 30 MHz. The TEM cell component of a hybrid RC/TEM facility is required to operate up to this frequency to provide continuous access to the RF spectrum. The field profile of the DSTO TEM cell scaled up to its intended size is shown in Figure 3.3. In Section 2.4, the proposed solution is documented to reduce the influence of the cavity resonances seen in Figure 3.3. These resonances limit the useable frequency of the TEM cell and so prevent the continuity between RC and TEM operation.

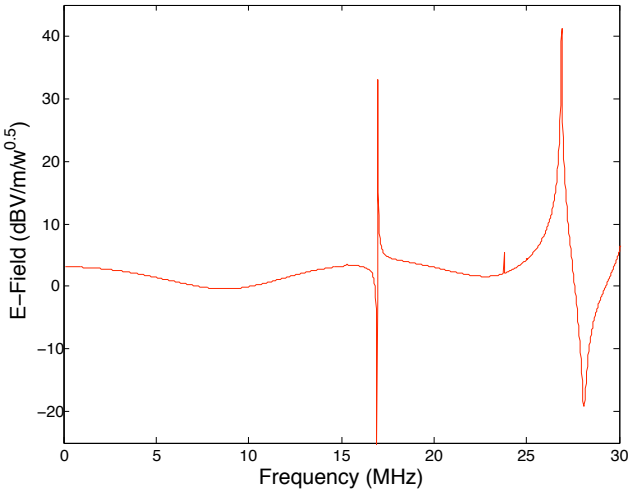

Figure 3.3: *Electric field profile for the DSTO TEM cell when scaled up to its intended size. Shown is the two cavity resonances which limit the useable frequency range of the cell.*

In Section 2.4 the TE_{011} resonance (17 MHz peak in Figure 3.3) was attenuated using active cancellation through a negative feedback system. Over 15 dB of attenuation was achieved. It is envisaged that similar performance could be possible when attempting to cancel the second more complex mode in Figure 3.3 at 27 MHz.

The feedback system designed to cancel the TE_{011} resonance is shown in Figure 2.48. It is unlikely that the feedback chain of amplifiers and filters will have to be changed when set-up to cancel the 27 MHz resonance. The difference will be in the placement of the half-loop antennas which will be orientated specific to the resonance. This may require there to be two sets of antennas one set for each resonance. This is not seen as a draw back due to the small number of resonances which need to be cancelled.

For a septum input power of 10 kW the feedback power amplifier must have an output of 720 W in order to cancel the resonance. A 1 kW amplifier which operates from 1-30 MHz with over 40 dB of gain would fulfil the requirement. This form of power amplifier is readily available from RF equipment stockists. Usually the narrower the frequency range of operation the cheaper the unit is. These power requirement figures are however, based on the concept demonstrator described in Section 2.4. With the use of tuned circuits, better impedance matching to the half-loop antennas could be achieved increasing the

efficiency of the energy transfer therefore requiring less power from the power amplifier.

As discussed in Section 2.4, the active cancellation system can become an oscillator if it moves into an unstable mode of operation. This would likely to be the result of the incorrect combination of the feedback signal's phase and gain. In this situation the fields inside the TEM cell could far exceed those expected and therefore have the potential to damage the equipment-under-test (EUT). As a safeguard the E-field inside the RC/TEM could be monitored by a system set-up to shut off the active cancellation power amplifier if a set field strength is exceeded.

Alternative means of dealing with the resonances include stepping over them in the test sweeps, or tuning them to different frequencies and running a second stepped sweep to cover the spectrum stepped over in the first sweep.

3.3 Costing

The preceding sections have discussed possible solutions for the integration of a TEM cell into the DSTO RC creating a RC/TEM hybrid testing facility. The intention of this section is to provide rough figures on the costing of these designs. Below is a table which lists the equipment required for the RC/TEM designs and the associated costs.

Table 3.1: *Costing table for adding TEM operation to the DSTO RC*

Item	Suplier	Model No.	Power	Frequency	Qty	Cost
			kW	MHz		AUD
Amplifier (Septum)	Faraday	10000A250	10	0.1-250	1	709,000
Amplifier (Cancel)	EMPOWER	GCS1D2GUT	1	1.5-32	1	28,000
Load (Solid Sept)	Electro Impulse	(RF) DACT-14	10	DC-30	1	2,500
Load (Wire Sept)	MicroOhm	RXLG-SI	1		11	5,000
Building & Materials	Multiple	—	—	—	—	50,000
Total Cost (Solid)						789,500
Total Cost (Wire)						792,000

The quotes obtained to populate the Cost column of Table 3.1 are by no means exhaustive, but are intended as a guide only. The result suggests that for either of the septum designs the integration of a TEM cell into the DSTO RC could cost approximately $800,000. The major cost driver within this price is the 10 kW power amplifier required to generate full level test fields. Less power could be used to drive the septum and hence produce a lower test field but for a lower equipment cost. However, for lower field levels the testing would need to be carried out in combination with BCI, negating some of the advantages that using solely the TEM cell provides. It would still provide some advantages over low level swept measurements on an OATS: protection from the weather; secure test environment; and no need for multiple antenna locations.

For hybrid RC/TEM designs of different scales and proportions to that at DSTO, the principle may be applied that all powers scale according to the cross section area transverse to the TEM propagation. The present RC/TEM design has a cross section of 11 m $\times$ 6 m

= 66 m^2. An RC/TEM design of cross section 20 m × 6 m = 120 m^2 would require a power for the septum of (120/66) × 10000 = 18 kW to reach a field level of 100 V/m.

References

1. Carter, N. J. (2003) The past, present and future challenges of aircraft emc, *IEEE International EMC Symposium 2003 proceedings.*

2. *Guide to Certification of Aircraft in a High Intesity Radiated Field (HIRF) Environment* (2000) SAE ARP5388, SAE International.

3. *The Certification of Aircraft Electrical and Electronic Systems for Operation in the High Intensity Radiated Field (HIRF) Environment* (2000) Advisory Circular 20-HIRF, FAA.

4. Crawford, M. L. (1974) Generation of standard em fields using tem transmission cells, *IEEE trans. on EMC.*

5. Carbonini, L. (2001) A new transmission-line device with double-polarization capability for use in radiated emc tests, *IEEE trans. on EMC* **43**(3), 326.

6. Monahan, R. L., North, T. M. & Xiong, A. Z. (1999) Characterization of large tem cells and their interaction with large dut for vehicle immunity testing and antenna factor determination, *Proceedings IEEE EMC Symposium Seattle Aug 2-6* p. 245.

7. Carbonini, L. (1992) A sielded multi-wire transmission line for susceptibility measurements with horizontally polarized electric field, *8th International Conference on EMC Sept. 21-24* pp. 33–38.

8. Crawford, M. L., Ma, M. T., Ladbury, J. M. & Riddle, B. F. (1990) Measurement and evaluation of a tem / reverberating chamber, *NIST Technical Note 1342 United States Department of Commerce.*

9. Lehman, T. H., Freyer, G. J. & Crawford, M. L. (1997) Recent developments relevant to implementation of a hybrid tem cell/reverberation chamber hirf test facility, *Digital Avionics Systems Conference 1997* **1**, 4.2–26.

10. Kempf, D. R. (1997) A proposed hirf test facility for aircraft testing, *Digital Avionics Systems Conference 1997* **1**, 4.2–22.

11. (n.d.). FEKO, EM Software and Systems-S.A. (Pty) Ltd, http://www.feko.info.

12. Leat, C. (2005) Understanding skin current distributions on an aircraft at hf using eigencurrent expansions, *in IEEE International Symposium on Electromagnetic Compatibility, Chicago*, Vol. 2, pp. 426 – 431.

13. Lorch, R. & Mönich, G. (1996) Mode suppression in tem cells, *IEEE International Symposium on EMC 19-23 Aug* pp. 40–42.

14. Hill, D. A. & Walsh, J. A. (1983) Resonance suppression in a tem cell, *Journal of Microwave Power* **18**(4), 325.

15. Carbonini, L. (1993) Comparison of analysis of a wtem cell with standard tem cells for generating em fields, *IEEE trans. on EMC* **35**(2), 255.

16. Klinger, M., Egot, S., Ghys, J.-P. & Rioult, J. (2002) On the use of 3-d tem cells for total radiated power measurements, *IEEE trans. on EMC*.

Appendix A Matlab Code

```
% This file calculates the loop gain for the TEM cell feedback profile.
% It then tests the Nyquist criterion ie. BA<1 for stable feeback.
% In cases where BA>1 the feeback system becomes an oscillator. This is
% what we want to identify and avoid.

% Load in TEM cell current feedback profile.
fid = fopen('FDAT1_1.BIN')
fid2 = fopen('FDAT2_1.BIN')
ml=fread(fid,'float','s');
pl=fread(fid2,'float','s');
magnitude_loop = 10.^(ml./20);
phase_loop =pl;
Z = magnitude_loop.*exp(i*phase_loop*pi/180);
B=-1.*Z;

% gain index for the BA matrix
indexA=0;

% This sets up the BA matrix will every entry set to 1.
BA(1:121,1:360)=1;

for A = 0:0.5:60 % this loop sets the gain
    indexA=indexA+1; % gain index
    Gain_is=A % used as a progess indicator on the screen
    index_is=indexA % another progress indicator
    magA=10^(A/20); % convert gain to linear
    for theta = 1:360 % set phase angle
        % combine phase angle and gain to form complex number.
        A=magA*exp(i*theta*pi/180);
        for freq_index = 1:1201 % step through the Feko frequencies.
            BA_val=B(freq_index)*A; % calculate BA (loop gain).
            BA_mag=abs(BA_val); % magnitude of BA
            BA_phase=angle(BA_val)*(180/pi); % phase of BA
            if BA_mag >= 1.0 % Nyquist criterion.
                % This is a -+10% error margin for the phase angle.
                if (BA_phase <= 170.0) & (BA_phase >= -170.0)
                    % identifies unstable feedback point.
                    BA(indexA,theta)=0.5;
                end
            end
        end
    end
end

% Plot results.
y=0:0.5:60;
x=1:360;
imagesc(x,y,BA)
title('Feedback Loop Stability Plot')
xlabel('Phase Angle (degrees)')
ylabel('Voltage Gain (dB)')
map=hsv(2)
colormap(map)
```

DEFENCE SCIENCE AND TECHNOLOGY ORGANISATION DOCUMENT CONTROL DATA	1. CAVEAT/PRIVACY MARKING

2. TITLE	3. SECURITY CLASSIFICATION
Assessment of TEM Cells for Whole Aircraft EMV Testing	Document (U) Title (U) Abstract (U)
4. AUTHORS	5. CORPORATE AUTHOR
Andrew J. Walters and Chris Leat	Defence Science and Technology Organisation PO Box 1500 Edinburgh, South Australia 5111, Australia

6a. DSTO NUMBER	6b. AR NUMBER	6c. TYPE OF REPORT	7. DOCUMENT DATE
DSTO–RR–0149	013-897	Research Report	May 2007

8. FILE NUMBER	9. TASK NUMBER	10. SPONSOR	11. No OF PAGES	12. No OF REFS
2006/1110165/1	AIR 06/007	DGTA	67	16

13. URL OF ELECTRONIC VERSION	14. RELEASE AUTHORITY
http://www.dsto.defence.gov.au/corporate/reports/DSTO–RR–0149.pdf	Chief, Air Operations Division

15. SECONDARY RELEASE STATEMENT OF THIS DOCUMENT

Approved For Public Release

OVERSEAS ENQUIRIES OUTSIDE STATED LIMITATIONS SHOULD BE REFERRED THROUGH DOCUMENT EXCHANGE, PO BOX 1500, EDINBURGH, SOUTH AUSTRALIA 5111

16. DELIBERATE ANNOUNCEMENT

No Limitations

17. CITATION IN OTHER DOCUMENTS

No Limitations

18. DSTO RESEARCH LIBRARY THESAURUS

Avionics Electromagnetic environments
Electromagnetic compatibility Testing

19. ABSTRACT

Transverse Electromagnetic (TEM) cells offer one solution to the problem of electromagnetic vulnerability (EMV) testing of whole vehicles at lower frequencies. Combined with a reverberation chamber (RC) TEM cells offer an attractive solution to a EMV testing facility which could operate in the frequency range of 10 kHz to 18 GHz. In order to move toward a hybrid RC/TEM facility the non-uniform transition region between TEM and RC operation (i.e. 17 MHz to 30 MHz) must be addressed. This report discusses computational electromagnetics (CEM) modelling used to characterise the DSTO scale TEM cell. The cell was built with the aim of integrating a full scale version into the DSTO RC. The CEM model of the TEM cell was validated using measurements, which showed good agreement. It was then assessed for applicability for aircraft EMV testing by comparing a simulated aircraft in the cell against an aircraft on an Open Area Test Site (OATS) and in free space. The work highlighted the need for resonance suppression in the transition region. We introduce a novel way of active resonance suppression and demonstrate its effectiveness when applied to the first TE resonance. Finally the feasibility of integrating a TEM cell into the DSTO RC is discussed including costs for major items